Annual Progress Report

for

NASA Research Grant NAG 1-443

entitled

"An In-Situ Study in SEM of Delamination in Several Graphite/Epoxy Composite Material Systems"

prepared by

Walter L. Bradley
Professor of Mechanical Engineering
Texas A&M University
College Station, TX 77843
409-845-1259

(for work completed from 2/1/85 through 5/31/86)

August 31, 1986

Contact Monitor: Dr. John Crews
NASA Langley

1.0 INTRODUCTION

The purpose of this report is to summarize research results completed in conjunction with NASA Research Grant NAG-1-443, for the time period February 1, 1985 - May 31, 1986. This report will be organized to be consistent with the original work statement of the grant proposal. Each of the original work statements will be indicated and then the research activities performed to accomplish the individual work statement items will be summarized.

2.0 SUMMARY OF ACCOMPLISHMENTS

2.1 In-Situ Fracture Observations

The original work statement item 2.1 indicated, "In situ fracture studies in the SEM will be performed to better define the deformation and fracture processes in mode I and mode II loading". The following has been done to accomplish the objective of this work statement.

2.1 DESIGN, CONSTRUCTION AND IMPLEMENTATION OF FIXTURES FOR MODE II DELAMINATION FRACTURE IN SEM

A new three point bend fixture compatible with our current loading stage for the SEM has been designed and fabricated. End-notched flexure tests have been run on several materials with typical results presented in Fig. 1. Now that this capability is established, mode II studies are under way on our model systems.

2.1.2 COMPARISON OF DEFORMATION/DAMAGE ZONE SIZES AND SHAPES FOR MODE I AND MODE II DELAMINATION FRACTURE

Work to date has been on AS4/3502, T6T145/F155, and T6T145/F185. The deformation/damage zone for mode II loading is long, and generally confined to the resin rich region between plies (see Figure 2). The composite seems to behave like two relatively rigid slabs with a much softer resin joining the two. The damage zone for mode I loading tends to be greater in height and shorter in width. Typical results for damage zone size for mode I loading are summarized in Table 1. Similar results for mode II loading will be obtained in the coming contract year. Fracture toughness measurements, G_{Ic}, are also included in Table 1. In general the correlation of damage zone size to mode I fracture toughness is quite good.

2.1.3 FRACTURE OF NEAT RESIN SPECIMENS IN SEM

We have recently begun to fracture neat resin specimens in the SEM. Typical results are seen in Figure 3. A paper in which the deformation/damage zone size for mode I fracture of neat resin is compared to that for mode I delamination of a composite made from the same resin has been submitted and accepted for publication in Polymer Science and Engineering. In this paper (see Appendix I) the decrease in delamination fracture toughness, compared to neat resin toughness, due to rigid fiber filler and interlaminar failure is addressed.

One of the problems associated with the observation of neat resin fracture in the SEM has been specimen preparation. The neat resin specimens used are approximately 2" long, 1" wide and .1-2" thick. Obtaining a uniform polish and maintaining specimen flatness has been particularly difficult on relatively soft resins such as polycarbonate. To solve this problem we have recently purchased with

State of Texas monies a $12,000 Struers microprocessor controlled polishing unit. This machine has greatly improved the quality and ease of specimen preparation.

2.1.4 INTERPRETATION OF APPARENT MICROCRACKING IN NEAT RESIN SPECIMENS

Previous work on the fracture of neat resins specimens in the SEM produced microcracking on such a fine scale that it was unclear whether these microcracks originated in the 100A thick sputter coated gold/palladium film applied to minimize charging or in the resin specimens (see Figure 4). This is in contrast to the microcracks observed during delamination of composites which clearly seem to be real microcracking in the composite (see Figure 5). An experimental program was designed to try to determine the proper interpretation for these cracks. This program consisted of observing SEM coated specimens of rubber which were first stretched to various strain levels prior to the sputter coating with Au/Pd to a thickness of 100A (series #1). A second series of experiments were also run in which specimens of rubber were first coated and then stretched and observed in the SEM (series #2). The series #1 of experiments allowed the determination of what, if any damage the rubber experienced for various degrees of stretching. Typical results are seen in Figure 6 and were further confirmed with a limited number of observations on uncoated, stretched rubber. Except for small, local voiding, no significant damage was noted, even at strains of up to 30%.

The intention of the series #2 experiments was to determine the

threshold strain level at which film microcracking begins and (if it does occur) the appearance of the film, or coating microcracks. The comparison with observations on uncoated specimens and specimens stretched before coating (series #1 experiments) was included to be certain that we could distinguish microcracking artifacts in the film from artifacts formed in the rubber itself during stretching. Even though no significant damage to the rubber was expected in the strain range used, it was nevertheless important to verify that this was indeed the case.

The results of the series #2 tests are presented in the photographs shown in Figure 7, which should be compared to the series #1 results shown in Figure 6. The film microcracking is seen to initiate at a nominal (or average) strain of only 5%. It is possible that the strain distribution in the rubber is heterogenous, in which case the actual threshold value might be somewhat larger. In fact the distribution of the microcracking strongly suggests heterogeneous deformation. As the nominal strain increases, the density of the microcracking increases and the width opening of each microcrack also increases. The microcracks appear to nucleate at the inclusion particles in the rubber and quickly coalesce into the observed continuous cracks which run perpendicular to the loading direction.

In summary, we conclude from comparison of the results presented in Figures 6 and 7 that film, or coating microcracking does occur and can occur at strain levels as low as 5%.

To further confirm these findings, a second set of controlled experiments was run on Lexan (without copel rubber additions). A miniature compact tension specimen was fatigue precracked and then

loaded in displacement control until crack extension occurred. The specimen was subsequently coated and observed in the SEM without any reloading. The results are seen in Figure #8. A deformation zone or damage zone is clearly seen ahead of the crack tip. At high magnification, the surface is seen to have a "rumpled" appearance due to deformation. At a lower magnification it would be easy to misinterpret these artifacts as microcracks. A few real cracks are noted in Figure 8, and these are clearly distinct from the rumpling due to deformation.

Subsequently, a miniature compact tension specimen of Lexan was carefully polished, sputter coated with Au/Pd, and then loaded in the SEM. The results are presented in Figure 9 and should be compared to the results previously discussed in Figure 8. The high density of microcracking seen in Figure 9 but absent in Figure 8 is the result of coating microcracking. A few real cracks which have formed in the Lexan are also noted in Figure 9 and are easily distinguished from the more superficial coating microcracks.

The significance of these results are that the possibility of film microcracking must always be considered when interpreting fracture observations on surfaces which have previously been coated. However, one must not jump to the conclusion that all surface microcracks are in the coating.

To illustrate, compare the results for fracture of neat resin Hexcel F185 (Figure 4) to the results for the composite made from this resin T6T145/F185 (Figure 5). The high density microcracking with some indication of surface charging in Figure 4 should be interpreted

to be film cracking due to high local straining. The appearance of charging in these very fine cracks suggests subsurface nonconducting material in these cracks, which implies film cracking without surface resin cracking. The fact that the microcracked zone has the same shape as the plastic zone in metals further supports this interpretation. By contrast, the microcracks in Figure 5 (note it is at a much lower magnification) are much larger, less dense and without any indication of charging. In some cases, very fine, charged microcracks such as those seen in Figure 4 are found to grow, coalesce and develop the appearance of actual microcracks such as those seen in Figure 5. In such cases, a duplex appearance of fine, film microcracks and coarser resin microcracks is present on the specimen surface (see Figure 9). It should be noted that the actual microcracks (as distinct from the coating cracks) never have a distribution which mimics a plastic zone in metals, which is further evidence that these cracks are resin cracks and not just coating cracks due to resin deformation beyond some critical strain threshold.

The microcracking of the Au/Pd coating can be used to good advantage since it allows one to map the region around the crack tip that has exceeded some threshold strain (which we noted was approximately 5% for a 100-150A coating). In previous work we have only observed coating microcracking in the more ductile resin systems such as Hexcel F155 and F185 but not in Hercules 3502. This implies fracture in the more brittle resin systems at crack tip strains less than 5%.

2.1.5 IN-SITU FRACTURE IN SEM AND POST-MORTEM FRACTOGRAPHY OF

MODEL COMPOSITE SYSTEMS BASED ON LEXAN AND LEXAN WITH COPEL RUBBER

Post-mortem fractography and in-situ frature in the SEM have been used to determine the micromechanics of the fracture process in two model systems; namely, Lexan and Lexan with 10% copel rubber additions.

2.1.5.1 POST MORTEM FRACTOGRAPHY

The fracture surface of the delaminated AS4-W6/Lexan and AS4W6/Lexan-10% Copel composite systems are presented in Figs. 10-12. The general appearance of the fracture surface of AS4W6/Lexan (Figure 10a) indicates that the Lexan matrix undergoes considerable deformation prior to fracture.

Primary delamination crack propagation in the plane of the page occurs locally by the coalescence of microcracks that form due to deformation of the resin. The microcracks have a duplex distribution, as seen in Figures 10c and 10d. The fine microcracks form where the distance between adjacent fibers is small across the plane of cracking.(e.e.; where the resin rich region between plies is locally thin). Conversely, a thicker resin rich region between plies (locally) gives a coarser microcrack spacing and thicker scallops. It is also clear in Figure 10c that considerable deformation and rotation accompanies the formation of the scallops by microcrack coalescence.

It is apparent from the fractographs presented in Fig. 10, that the fibers are well wetted by the Lexan matrix, resulting in good fiber/matrix adhesion. The observation of good fiber/matrix adhesion

is further supported by the fact that a fairly small tie-zone was formed during mode I delamination, giving relatively little fiber breakage and pullout.

The copel rubber toughened AS4-W6/Lexan-copel composite, on the other hand, behaved quite differently. A rather large tie-zone was observed which continued to grow as delamination proceeded until a constant tie-zone size was achieved. Prior to this, fiber breakage was minimal. However, once the tie-zone reached its steady-state size, further crack propagation resulted in considerable fiber breakage. This is clearly evident in Fig. 11a. There is an abundance of loose fibers on the surface and, as Fig. 11b exemplifies, these loose fibers are rather poorly wetted by the resin. The surface of the fibers appears quite bare. This is typical of the fracture surface in general in this system (see fig. 12 a,b). Thus, it appears that the W6 epoxy sizing on the fibers provides for excellent adhesion with the Lexan but is quite ineffective when the Lexan is toughened with copel rubber.

A close examination of the fractography in Fig. 12b reveals some interesting features that may account for the difference in interfacial adhesion between the Lexan and the Lexan with copel rubber. The appearance of the resin on the fracture surface where resin/fiber debonding occurred is very foam-like and is quite different from the appearance of the regular Lexan when it debonds from the fibers (see Fig. 10b).

A detailed view of the foam-like regions is presented in Fig. 12c. The cavities are probably formed by the rupture of the dilated copel rubber phase. The rubber, with a much greater coefficient of

thermal expansion than the matrix will be quite dilated after the cool down to room temperature, and upon final rupture, collapses, resulting in the formation of cavities.

From the abundance of the cavitation at the fiber/matrix interface, it would appear that there must be preferential segregation of the rubbery phase to the fiber-matrix interface. This in turn results in a weaker interfacial bond.

A final interesting observation from this series is found in figure 12d, where the fractured surface of a T6T145/F185 composite is seen in a resin rich region. Note the very ductile behavior of the resin in the absence of fiber constraint and/or debonding. The much smaller amount of resin deformation which typically accompanies delamination fracture in this material accounts for the 2000 J/m^2 delamination G_{Ic} compared to an 8400 J/m^2 value for the neat resin.

2.1.5.2 IN-SITU IN SEM FRACTURE STUDIES

Mode I delamination of Lexan and Lexan with 10% copel rubber was observed in the scanning electron microscope under displacement controlled conditions, which permitted stable crack growth in these systems. Crack propagation occurred simultaneously in the interlaminar region and at an adjacent fibre matrix interface in the AS4-W6/Lexan system (see Fig. 13a). Here the interfacial debond crack lies behind the interlaminar crack. This was often reversed during the propagation of the crack, with the interlaminar crack sometimes ahead of and sometimes lagging behind the interfacial crack. This indicates that the interfacial fracture toughness is comparable to the

primary bond strength in the Lexan matrix (i.e., good interfacial bonding). The crack tip region, Fig. 13b, c, reveals some microcracking which does not extend over the entire width of the 100 μm wide interlaminar region. Partial coalescence of microcracks ahead of the crack tip is also discernible. A detailed view of the adjacent fibers (Fig. 13d) shows the formation of microcracks prior to their coalescence into a macrocrack (compare with Figure 10d).

The fact that crack propagation occurs through the matrix and at the matrix-fiber interface with about equal resistance in the Lexan without copel rubber confirms our earlier observation from the fractography section that the interfacial bonding in this system is generally good.

Figures 14 a-c are micrographs of the in-situ delamination of the AS4-W6/Lexan-Copel system. The interlaminar region is narrower than in the AS4-W6/Lexan system (about 30-50 μm versus 100 μm wide) and has a much more dense network of microcracks (Fig. 14b,c). Based on our earlier discussion of the results on rubber specimens, it would be appropriate to interpret the fine microcracks as film microcracks with the coarser microcracks as real resin cracks. If one thinks of the fine microcracks as an indication of strain and the coarse microcracks as resulting from local ductile rupture, then one can see how the fine microcracks lead to the coarser microcracks. Microcrack coalescence leading to crack microcrack propagation is very clearly exhibited in Fig. 14a-b. Finally the interfacial debond crack is well ahead of the interlaminar crack. This was consistently the case throughout the delamination of the AS4-W6/Lexan-Copel rubber composite, and at no time during the test did the interlaminar crack tip lead the

interfacial crack tip. This clearly demonstrates that the interfacial bond strength is relatively poor, as previously indicated from fractography and from the size of the fiber-bridged tie-zone observed during split laminate testing of full size specimens.

The heterogenous distribution of the copel rubber previously noted in the post-mortem fractography is deleterious for two reasons. The toughening it produces in the resin will be quite nonuniform and the segregation to the matrix/resin interface has been shown to weaken the interface.

2.2 STRAIN FIELD MEASUREMENTS AROUND CRACK TIP

The original work statement item 2.2 indicated, "Stereo-imaging will be utilized to determine the strain field around the crack tip". The following tasks have been performed to meet the objective of this work statement.

2.2.1 DEVELOPMENT OF STEREO-IMAGING TECHNIQUE

An experimental technique has been developed to measure in-plane strains using stereo-imaging. The details of this approach and some typical results obtained using equipment at Texas A&M University were previously presented in our semi-annual report, March 12, 1986.

2.2.2 VERIFICATION OF IN-HOUSE EXPERIMENTAL TECHNIQUE

The critical experimental step required to obtain accurate quantitative strain measures is the determination of the in-plane displacements using a special stereo-microscope to look at SEM

stereo pairs of the crack tip loaded and unloaded. The in-plane point displacements due to loading will appear in the stereo viewer as topography. The apparent topography can then be used to determine the in-plane displacements required to produce this apparent topography. These displacements can then be used to calculate strains.

Commercial equipment used for aerial mapping can quantify the in-plane displacements very precisely, but such equipment costs $250,000. Thus, we have been experimenting with less sophisticated equipment available at TAMU to see if we can still obtain reasonable accurate quantitative results, since commercial results cost $4.00/point. We have analyzed results from one mode II test using our equipment and have had a commercial company in San Antonio check the results presented in our semi-annual report, March 12, 1986. This comparison indicated that our determination of in-plane displacements on our in-house equipment were approximately correct, but with an error of ±20% of the absolute values measured.

2.3.3 DIRECT STRAIN FIELD MEASUREMENTS IN SEM

We are now exploring an alternative approach to stereo imaging to measure strain fields around crack tips. This approach involves vapor deposition over a mask (or template) with suitably spaced holes (square grid with 1μm spacing). A coarser mask will be prepared using a laser and then be reduced using a photo-reducing technique developed for and utilized in the electronics industry.

Specimens with the grid applied will be photographed unloaded and loaded in the SEM. A standard image analyzer will be used to calculate the displacement field of the various grid points. A

computer program will be used to convert the two displacement fields into strain fields. This technique should give better precision and better resolution for our measurement of strain fields around crack tips than our current stereo imaging technique does.

2.3 The third portion of the proposal work statement for NAG-1-443 indicates "Further refining of testing and analysis techniques for mode I and mode II delamination of split laminates will be performed". The following effort is in progress to meet the requirements of this work statement.

2.3.1 COMPARISON OF END-NOTCHED FLEXURE TEST AND END-LOADED FLEXURE TEST

Street and Russell (2) introduced the end-notch flexure test for pure mode II testing of split laminates about the same time Bradley and Vanderkley (3) introduced the end-load flexure test (see Figure 15). Tests have recently been completed to determine whether these somewhat different loading arrangements for split laminates give consistent values for G_{IIc}. These results are summarized in Tables II and III, with the data analysis being conducted by three different methods. The area method is the most general approach allowing for geometric nonlinearity, but assumes all energy dissipation is occurring in the crack tip region. For a linear load-displacement curve, the area method and the linear elastic analysis results are consistent. For a nonlinear load-displacement curve, the linear elastic analysis gives artifically high indications of G_{IIc}.

The important result from Tables II and III are that the two methods give consistent indications of G_{IIc} when the experimental results are properly analyzed (i.e., when the area method is used for nonlinear elastic behavior). The results also illustrate the erroneous results one obtains when a linear analysis is used for moderately nonlinear load-displacement behavior.

2.3.2 RECENT RESULTS OF MODE I AND MODE II TESTS ON MODEL SYSTEMS

Fracture toughness measurements and in-situ fracture studies have been conducted on the following composite systems: (1) AS4-W6/Lexan; (2) AS4-W6/Lexan-10% Copel; (3) AS4/PEEK-APC-2; (4) BP 907/T300; (5) T6T145/F185; and on the matrix resins Lexan and F185. The composites were tested for Mode I and Mode II opening delamination toughness using DCB specimens from undirectional laminates 24 plies thick, with Kapton inserts as crack starters. Specimen geometries for mode I and mode II opening are shown in Fig. 15. The load-displacement record was obtained directly from the MTS servohydraulic frame in the form of an x-y plot and was also simultaneously digitized via an HP 3497A data acquisition system, and subsequently, stored through an HP9122 desktop computer. Crack lengths at successive unloads were measured visually.

The area method was used to obtain delamination G_{Ic} and G_{IIc} values because the load-displacement record was too nonlinear to justify the use of linear beam theory analysis (see Figures 16-21). In the case of the AS4/PEEK APC-2, discontinuous, or unstable crack growth was noted in mode I. Thus, the area method gives an average value between initiation and propagation G_{Ic} values.

As an alternative to the area method analysis for mode I delamination in PEEK where unstable crack growth occurred, a 5% secant offset approach was used to approximate the load-displacement values at the moment of initial crack extension for each reload. Since there was minimal nonlinearity at these points in the reload, linear beam theory analysis was used to calculate G_I, which was then assumed to be the initiation G_{Ic} value. The values so obtained were much higher than those obtained using the area method on the same data, which is undoubtedly a result of the fact that the initiation G_{Ic} is much greater than the unstable crack propagation "G_{Ic}" in PEEK. This implies the rate dependence in resistance to crack propagation is primarily in the rate dependance of the amount of energy absorption in the process zone. To put it another way, the energy absorbed decreased with increasing rate of crack propagation. This change in fracture energy with crack growth rate is consistent with the change in fracture surface features noted when the crack initiation portion of the fracture surface is compared to the crack propagation portion of the fracture surface (see Figure 22). All of the experimental results are summarized in Table IV.

2.3.3 FINITE ELEMENT ANALYSIS OF CRACK TIP STRESSES FOR ASYMMETRICALLY LOADED SPLIT LAMINATES

Vanderkley (3) has previously shown how one may calculate the G_{Ic} and G_{IIc} values for an asymmetrically loaded split laminate (the limiting case of which is the end loaded flexure test). Nevertheless a more detailed analysis of the state of stress at the crack tip is

needed to define the conditions under which the delamination occurs for mixed mode I and mode II loading. A finite element program has been adapted for this purpose.

The stress field ahead of the crack tip of a split laminate specimen loaded under mode I and mode II delamination conditions has been determined by means of this finite element analysis. The results have been compared to the observed damage zone developed ahead of the crack tip for the same loading conditions.

The determination of the stress field ahead of the crack tip of the split laminate specimen loaded under mode I and mode II was accomplished by first generating a two dimensional mesh 15.24 cm long and 0.254 cm thick consisting of 791 nodes and 294 elements. Triangular six-noded elements around the crack tip with mid-side nodes displaced to the quarter point [4], and a substantial refinement of the mesh around the crack tip were used to overcome the difficulty imposed by the stress singularity present at the crack tip. This was a linear analysis made with a finite element algorithm developed by Henriksen [5]. The algorithm is based on a nonlinear code updated with Lagrangian formulation using six and or eight noded isoparametric elements with two degrees of freedom per node. Typical properties of undirectional AS4/3502 graphite/epoxy composite were used in the analysis. Stress contour plots were obtained from the output data. Also, the stress distribution was plotted as a function of distance ahead of the crack tip.

Split laminate specimens 3.81 cm long, 0.508 cm wide and 0.114 cm thick, and 3.048 cm long, 0.508 cm wide, and 0.114 cm thick, of Hercules undirectional AS4/3501-6 graphite/epoxy were used for mode I

and mode II observations of the damage zones, respectively. The observations were done during real-time delamination in the scanning electron microscope. Mode I delamination was achieved by pushing a wedge into the precracked portion of the longer split laminate specimens, using the tensile stage in the scanning electron microscope. The wedge was sufficiently blunt to ensure that it remained well away from the crack tip, giving essentially pure mode I loading. Mode II delamination was achieved by means of a specially designed three point bend fixture installed to the tensile stage of the scanning electron microscope. The observations were performed in a JEOL JSM 35 scanning electron microscope. All surfaces observed were coated with a 100A thick good/palladium film to minimize charging effects associated with the nonconductive nature of the epoxy matrix of the composite. The experimental results were recorded on standard tri-x film.

Figure 23 shows the finite element results of a split laminate beam specimen tested under mode I delamination. Figure (23a) is a stress contour plot from the vicinity of the crack tip. Note how the stress is seen to rapidly decrease ahead of the crack tip. Figure (23b) shows the stress field distribution ahead of the crack tip normalized to the thickness 2h of the specimen. As can be observed, a pure tensile stress develops at the crack tip in the plane of delamination. The tensile stress rapidly drops off over a distance of 0.762 mm ahead of the crack tip where it actually goes into a compressive stress. Then, it slowly reached a maximum compressive stress level of approximately 7% of the maximum tensile stress

calculated to exist in the vicinity of the crack tip. Finally, it gradually approaches a zero stress level at a distance of about 7.62 mm from the crack tip. It should be noted that the compressive stresses observed are not expected to significantly influence the fracture mode at the crack tip because it develops far enough away from the crack tip.

Figure 24 shows the stress contour plot and stress field distribution in the vicinity of the crack tip of a split laminate beam specimen subjected to a pure mode II delamination loading. The shear stress drops off much more slowly with distance from the crack tip than does the normal stress for pure mode I delamination (compare Figures 23 and 24). Furthermore, the shape of the stress field is more narrow and elongated than for mode I. Figure (2b) shows the stress field as a function of distance ahead of the crack tip normalized to the thickness 2h of the specimen. The shear stress can be seen to monotonically decrease to a constant value of approximately 0.1% of the maximum load predicted at the crack tip, extending all the way to the end of the beam. The slower decreasing rate of the shear stress is in good agreement with the elongated shape of the shear stress contour seen in Figure (24). This indicates that the stress concentration at the crack tip is distributed over a larger range with the extent of the highly stressed material above and below the center plane being much smaller than for mode I.

Figure 25 corresponds to real-time observations of the damage zone developed ahead of the crack tip under mode I delamination of AS4/3501-6 graphite/epoxy. This damage zone is characterized by extensive microcracking of the resin extending at least 90 μ m ahead

of the microscopic crack tip and approximately 10-15 μm wide. Figure 26 shows the damage zone developed ahead of the crack tip under mode II delamination of AS4/3501-6 graphite/epoxy. In this case, the damage zone extends much further ahead of the crack tip (at least 270μm m) than the damage zone observed for mode I loading, and is only approximately 2.5-5 μm wide.

A careful comparison of the stress fields of Figures 23 and 24 and the damage zones shown in Figures 25 and 26 for mode I and mode II delamination, reveals a direct correspondance betwen them. The gradual decrease in the magnitude of the shear stress with distance from the crack tip for mode II (Figure 24b), along with the elongated shape of the shear stress contour plot seen in figure (2a) indicates that the stress concentration at the crack tip is distribution over a larger range, causing the size of the damage zone ahead of the crack to extend over a long range (Figure 26). In contrast, the rapid decay of the magnitude of the normal stress with distance from the crack tip for mode I loading (Figure 22b) and the more circular shape of the normal stress contour plot (Figure 22a), indicate that the stress concentration at the crack tip is much more localized, causing the size of the damage zone to be smaller than for mode II delamination (Figure 25). Furthermore, the extent of the stressed material above the center plane seen in the stress contour plots is much smaller for mode II than for mode I. Thus, the damage zone (Figures 25 and 26) changes from wide to narrrow as one goes from mode I to mode II. These findings indicate that the increased resistance to delamination going from mode I to mode II, especially for the more

brittle systems [6], has a direct relationship to the extent and rate of change of the stress field as well as to the extent and shape of the damage zones.

It should be noted that even though the finite element analysis assumed global linear elastic material behavior, it still predicted the overall trend in damage zone size and shape, despite the actual nonlinear behavior of composites in the crack tip region.

In summary, it has been found that the different size and shape of the damage zone observed when comparing mode I to mode II delamination is consistent with the difference in the size and shape of the stress field predicted by the finite element analysis. Furthermore, these differences are also consistent with the difference in resistance to delamination of brittle graphite/epoxy composites for the two types of delamination studied.

2.3.4 DETERMINATION OF STABILITY CONDITIONS FOR END-LOADED FLEXURE TEST FOR SPLIT LAMINATES

The end loaded flexure test has been analyzed to determine the degree of stability for crack growth as compared to the end-notched flexure test where stability is sometimes a problem. This has been done using linear beam theory. The results are presented in a dimensionless format in Figure 27. The conclusion reached is that an a/L value of approximately 0.5-0.55 should be ideal for achieving stable crack growth.

This analysis has been used to advantage in our experimental work. If a relatively long specimen with a short starter crack is used, the uncracked end of the specimen (See Figure 15) should be supported

initially at a location only a few inches from the crack starter end of the specimen. As the crack grows, this support position can be adjusted periodically to keep the a/L value in the vicinity of 0.5 The result has been the capability of measuring G_{IIc} numerous times on one specimen.

2.3.5 DEVELOPMENT OF A J-INTEGRAL ANALYSIS FOR USE ON SPLIT LAMINATES

The use of tougher resin composites and the need to test multidirectional layups will eventually preclude the exclusive use of a G_{Ic} type analysis, which is used almost universally to calculate delamination fracture toughness for delamination of split laminates. For situations where the load-displacement curve is nonlinear due to far field damage, one cannot use linear beam theory or the area method to obtain meaningful indications of the crack tip energy dissipation per unit area of crack extension.

Work done in conjunction with Dr. Richard Schapery has resulted in a derivation of the J value for a split laminate. The result is as follows:

where B = specimen width

k = curvature of beam

M = moment at the crack tip

Experimental work to verify that this does give a geometry independent prediction of delamination crack growth is now in progress. This work involves delamination studies of split laminates with many ±45° plies to reduce stiffness and increase the potential for far field damage.

So far, the specimens tested have only manifested geometric nonlinearity but not significant far field damage, or material nonlinearity. A geometry independent J_{Ic} has been found for this case for Hexcel T6C 145/F155. The more critical test, however, will be a geometry independent J_{Ic} determination for specimens with significant far field damage. Such specimens are currently being prepared for study.

2.3.6 J-INTEGRAL MEASUREMENTS ON NEAT RESIN

The use of tougher neat resins such as polycarbonate preclude the use of linear elastic fracture mechanics. The use of razor blades in such ductile test materials is also suspect. Thus, we have been doing development work to determine whether fatigue precracking is necessary. We have also been doing single and multiple specimen tests according to ASTM-E813-81 to determine whether any modifications of this approach developed for metals is in order for tougher polymeric materials. We have also been varying the displacement rate by a factor of 100X to determine the strain-rate sensitivity. This "shakedown" work has been performed on polyethylene since a limited amount of our model material polycarbonate, with and without copel rubber, is available. Typical results for polyethylene are seen in Figure 28.

3.0 SUMMARY OF PUBLICATIONS AND PRESENTATIONS PERFORMED IN CONJUNCTION WITH NAG-1-443 IN 1985

The following papers and presentations have been made possible in whole or in part by support provided by NAG-1-443.

3.1 W. Jordan and W. L. Bradley, "Micromechanisms of Delamination Fracture in Toughened Graphite/Epoxy Laminates", ASTM Symposium on Toughened Composites, Houston, TX, March 1985.(accepted)

3.2 M. Tse, M. Hibbs and W. L. Bradley, "Delamination Fracture Studies of Some Toughened Graphite/Epoxy Composites, Including Real Time Observation in Scanning Electron Microscope", ASTM Symposium on Toughened Composites, Houston, TX, March 1985. (accepted)

3.3 W. Jordan, M. Hibbs and W. L. Bradley, "The Meaning and Significance of Hackles in Composite Materials Failure Analysis", Proceedings of International Conference on Post Failure Analysis Techniques for Fiber Reinforced Composites, Dayton, Ohio, July, 1985, pp. 17-1 to 17-17.

3.4 E. Chakacherry and W. Bradley, "A Comparison of Crack Tip Damage Zone for Hexcel F185 Resin and T6T145/F185 Composite", presented as invited paper at ACS International Symposium on Nonlinear Deformation, Fatigue and Fracture of Polymeric Materials, accepted for publication in Polymer Science and Engineering.

3.5 M. F. Hibbs and W. L. Bradley, "Correlation Between Micromechanical Failure Processes and Delamination Fracture Toughness of Graphite/Epoxy Systems", Symposium on Fractography of Modern Engineering Materials, Nashville, TN, November 1985. (in review)

3.6 W. L. Bradley, invited lecture for Gordon Research Conference on Composite Materials, Santa Barbara, CA, January 1986, "Direct Observations of Delamination Fracture Processes".

3.7 W. L. Bradley and W. M. Jordan, "The Relationships Between Resin Ductility and Composite Delamination Fracture Toughness", Proceedings of International Symposium on Composite Materials and Structures" (Beijing, China; June, 1986), pp. 445-450.

4.0 OTHER REPORTS - The five month report of highlights of NAG-1-443 was submitted, June, 1985 to NASA. A Semi-Annual Progress Report for NASA Research Grant NAG 1-443 was submitted on March 12, 1986.

REFERENCES

1. J. G. Williams, Discussion at the ACS Symposium on Non-Linear Deformation, Fatigue and Fracture of Polymeric Materials, Chicago, September 1985.

2. A. J. Russell and K. N. Street, Delamination and Debonding of Materials ASTM STP 876, pp 349-370.

3. P. S. Vanderkley, Master's Thesis, Texas A&M University, December 1982.

4. Barsoum, R. S. "on the Use of Isoparametric Finite Elements in Linear Fracture Mechanics". International Journal for Numerical Methods in Engineering, Vol., 10 pp. 25-27, 1976.

5. Henriksen, M. Engineering and Physics Department, Colorado School of Mines, Golden, Colorado.

6. Jordan, W. M. "The Effect of Resin Toughness on Fracture Behavior of Graphite/Epoxy Composites", Ph.D. Dissertation, Texas A&M University, College Station, Texas, 1985.

Table I. Deformation/Damage zone sizes for composites; determined from in-situ fracture observations for mode I delamination fracture.

Composite System	Fiber density (vol. %)	Size of Damage Zone ahead of crack (m)	Size of Damage Zone above/below crack (m)	G
AS4/3502	76.4	20	5	190
F155 NR		20	7	335
T6T145/F155	59.6	30	20	1015
T6T145/F155	70.5	20	10	615
T6T145/F155	68.8	20	10	520
F185 NR		75	35	455
F185		200	50	2205

Table II. End-Loaded Split Laminate (ELS) Results.

Material	Specimen	Critical Load Pc (lbs)	Energy Absorbed (lb-in)		G_{IIc} (lb/in) I	II
AS4/3502	1	13.6	3.9		3.6	3.4
		11.1	2.9		3.5	3.2
		9.8	2.5		3.5	3.1
		8.9	2.5		3.7	3.1
	2	12.7	6.1		3.4	3
		9.1	3.1		3.4	3
		7.3	2.2		2.9	2.9
				Avg	3.4	3.1
T6C145/F185	1	46.8	9.9		*	12.3
		44.9	8.1		11.6	11.6
		42.3	6.9		13	13.8
		39.4	5.4		13	13.5
		36.5	4.8		12.5	10.7
		35.1	11		13	12.1
	2	46.6	7.7		11.2	15.1
		43.1	6.5		12.7	12.8
		41.4	6.7		13.8	11.9
		39.6	5		14.8	12.4
		38.4	8.9		15.5	15.8
		36.4	10.8		16	13.3
				Avg	13	12.9

* Nonlinearity is too great to satisfy linear beam theory assumptions implicit in this approach.

Table III. End-Notched Flexure (ENF) Test Results.

Material	Specimen	Critical Load (lbs)	Measured Compliance (in/lb x 10^{-4})	Energy Absorbed (lb-in)	G_{IIc} (lb/in) I	II	III
AS4/3502	1	125.6	6.2048	2.6	3	3.7	3.5
	2	125	6.1261	2.6	2.9	3.6	3.4
	3	137.5	5.9429	3	3.2	3.9	3.5
	4	131.5	6.0724	3	3.1	3.7	3.6
				Avg.	3.1	3.7	3.5
T6C145/F185	1	356.9	2.2715	7.8	* -	* -	12.8
	2	366.9	2.1017	10.7	-	-	15.4
	3	360	2.2443	11.7	-	-	14.2
	4	357.3	2.4753	9.3	-	-	11.4
				Avg.			13.7

* No calculation of G_{IIc} is possible due to significant nonlinearity in load/deflection curves. If one uses linear portion of curves to measure compliance and Pmax for crack extension (ignoring nonlinear behavior near Pmax), G_{IIc} lower bound values of 7 lb/in may be calculated.

Table IV. Fracture Toughness of Model Systems

Material	Neat Resin J_{Ic} (J/m^2)	Composite G_{Ic} J/m^2)	Delamination G_{IIc} (J/m^2)
T300/BP907	280	330[a], 370[b]	
AS4W6/Lexan	6100	685[c], 900[d]	*875-1000[c]
AS4W6/Lexan-10% copel	---	1170[e], 1800[f]	*1650-1800[e]
AS4/PEEK APC-2	---	1400-1850[x] 840-965[y] 1160[z]	3100

a 40.32% w/w resin
b different batch
c 41.8% w/w/ resin
d 42.95% w/w resin
e 36.6% w/w resin
f 39.8% w/w resin

x G_{Ic} for unstable propagation

y G_{Ic} for arrest see text for further details

z G_{Ic} from area method

* Values reported here are from most recent results and are different from those in the semi-annual report (March 12, 1986).

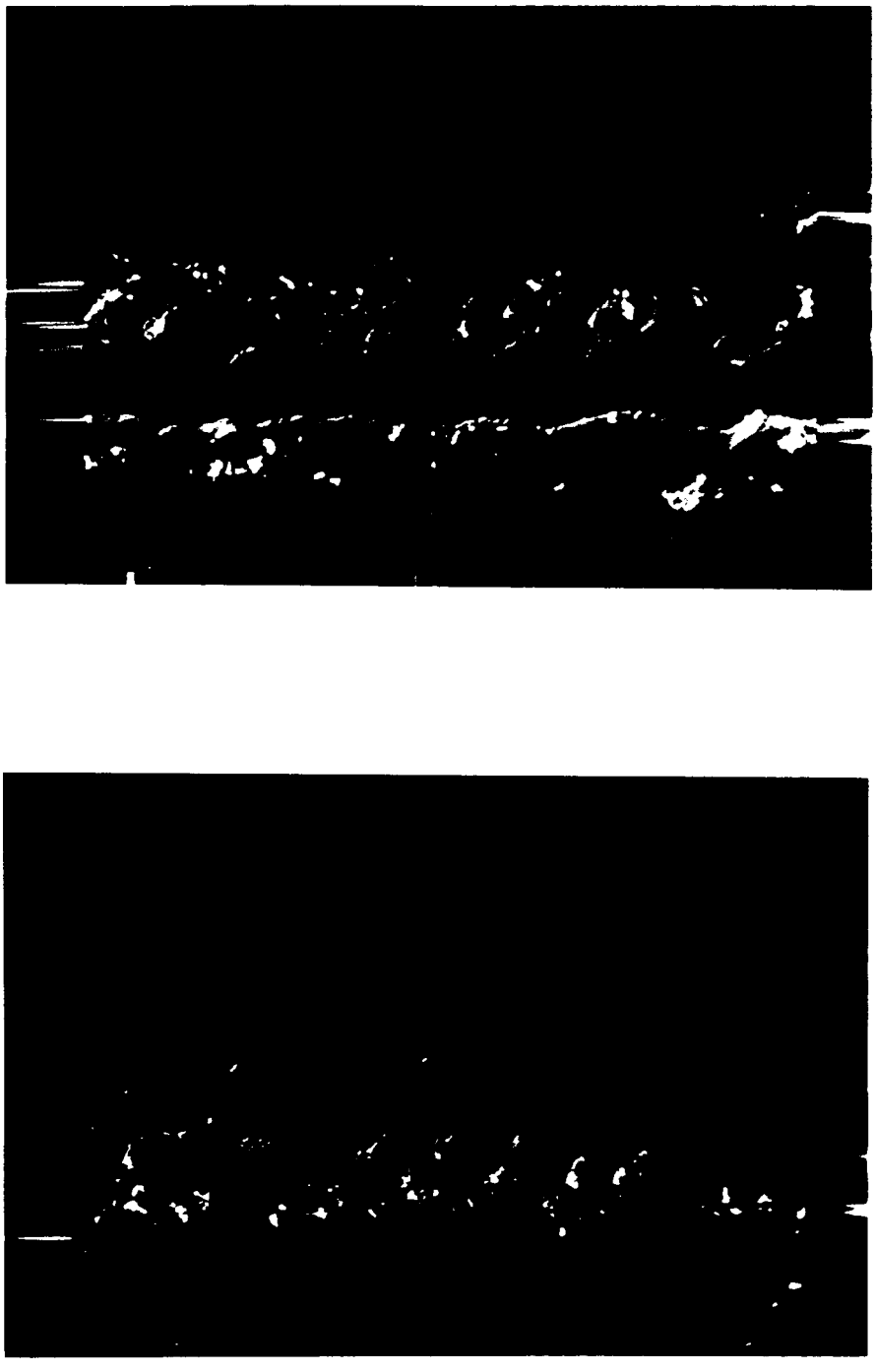

Figure 1. In-situ mode II delamination of AS4/3501-6 using an end-notched flexure fixture (2000X).

Figure 2. The damage zone ahead of the crack tip for a T6T145/F155 composite made from Hexcel prepreg and loaded in pure mode II. Note long narrow shape of damage zone.

Figure 3. In-situ mode I loading of F185 resin (3000X) with 150A thick sputter coating of a gold/palladium alloy.

Figure 4. In-situ mode I loading of F185 resin coated with Au/Pd film showing a dense network of microcracks around the crack tip which will be seen from the discussion to be mainly film microcracks rather than substrate microcrack. 4(a) 3000X 4(b) 5000X

Figure 5. In-situ mode I delamination of T6T145/F185 composite showing microcracking around the crack tip which is film and substrate microcracking. 850X

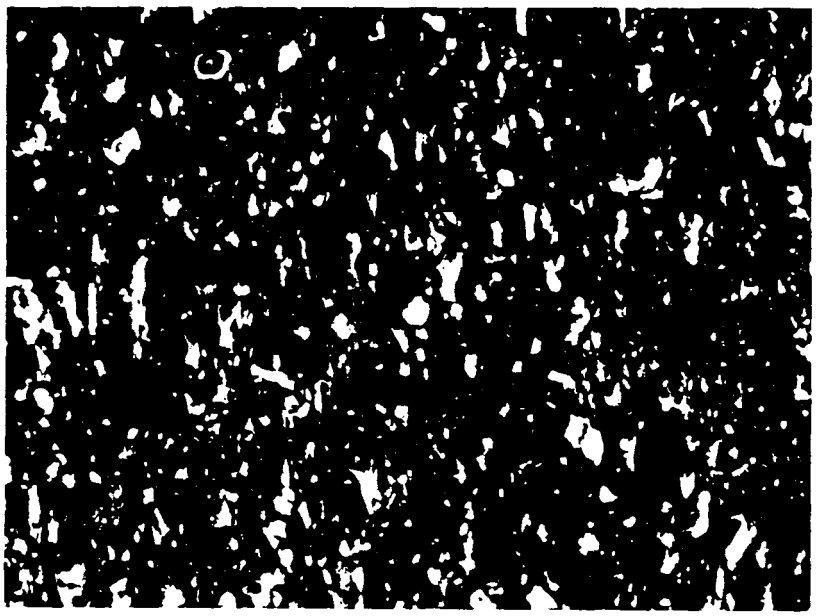

Figure 6. Rubber specimen that was stretched 30%, sputter coated while still stretched and then observed in the SEM, still stretched 30%. 1000X

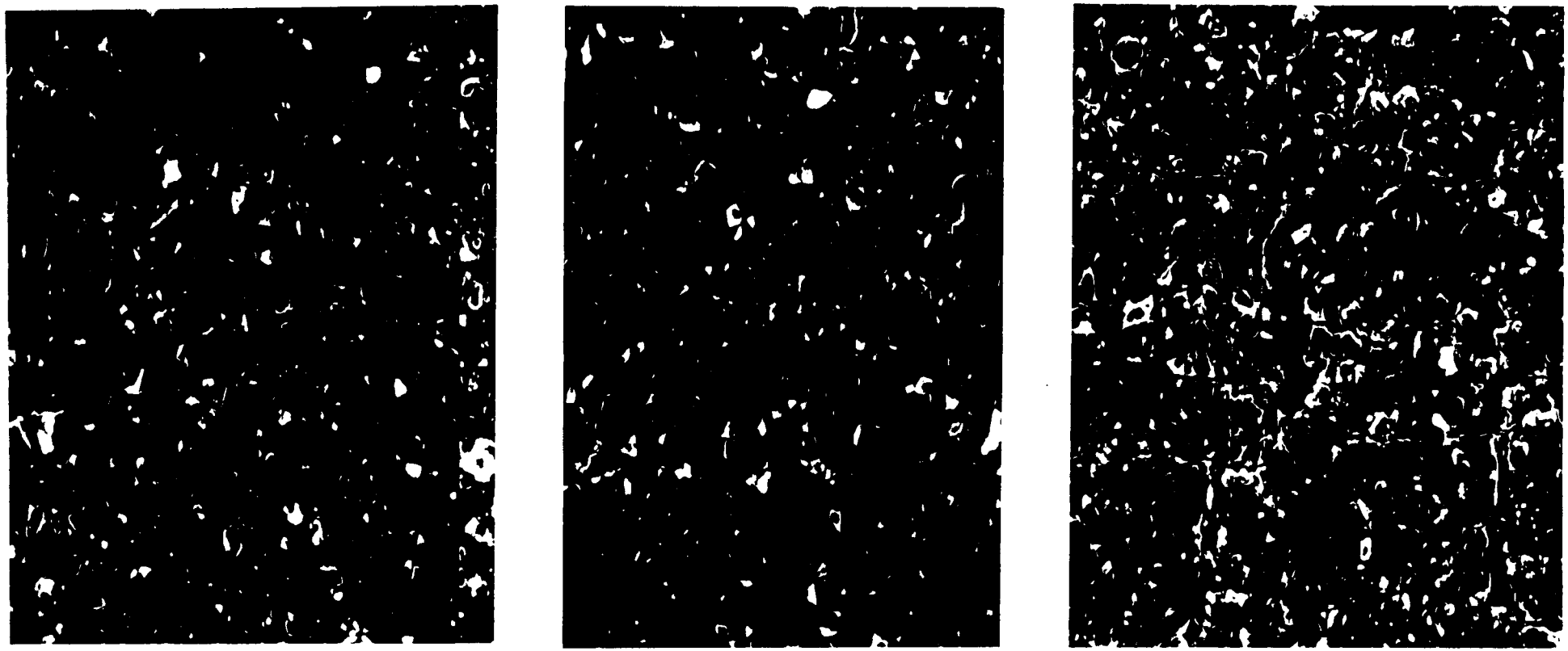

Figure 7. Rubber specimens that were coated and then stretched to varying strain values and subsequently observed in the SEM: (a) 0%; (b) 5%; (c) 10%; (d) 15%; (e) 35%; and (f) 50%, all at 1000X. Figure 7(g), strained 50% and photographed at 3000X. Well defined cracking in the coating but not in the subsurface rubber is seen.

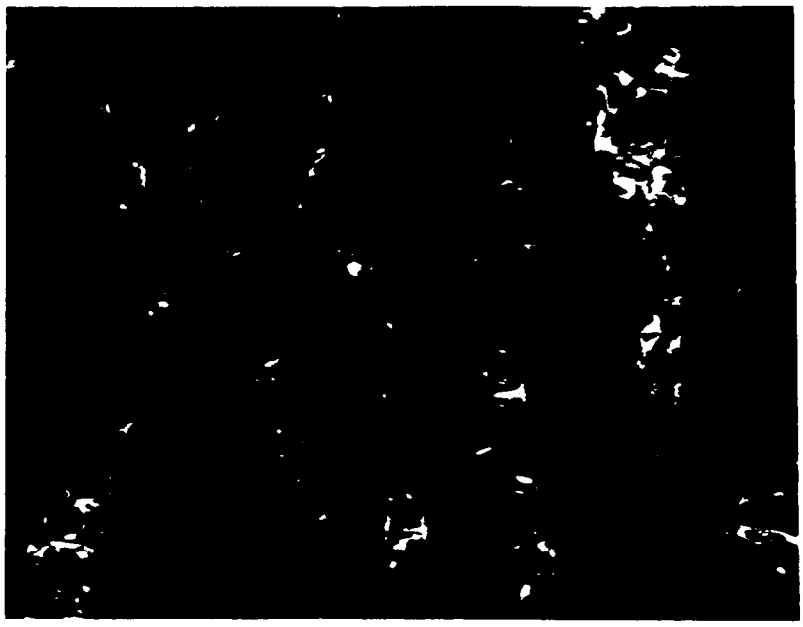

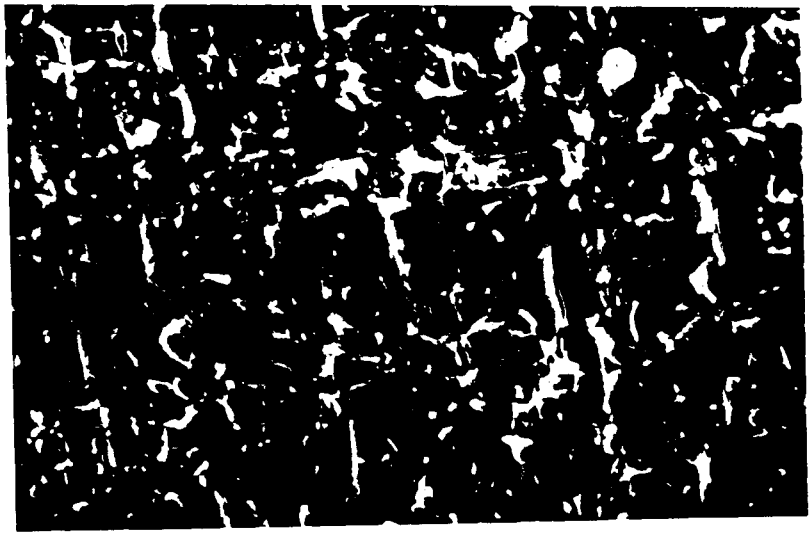

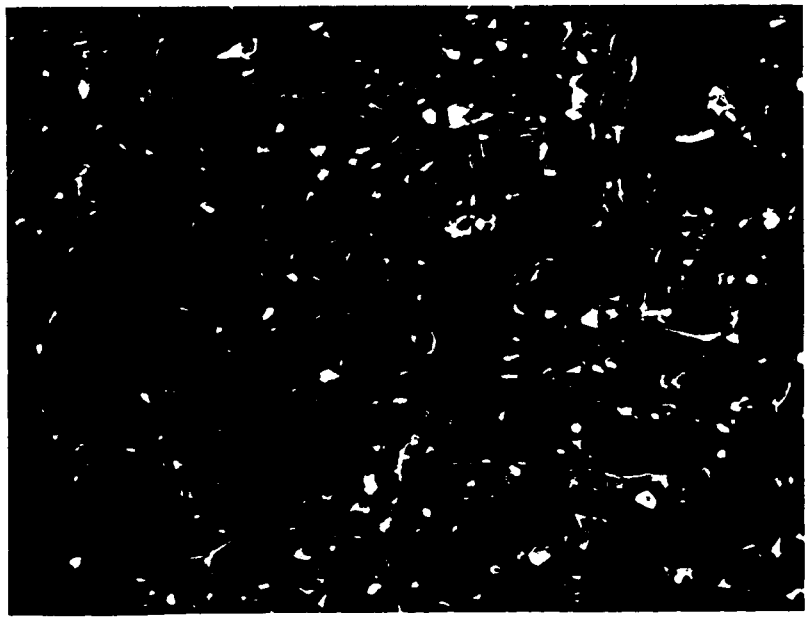

Figure 7(d), 9(e) and 9(f). (Caption on previous page).

Figure 7(g). (see caption on previous page)

Figure 8. Compact tension specimen of Lexan neat resin (without copel rubber), loaded in MTS, subsequently coated, and then observed in the SEM. Note the surface wrinkling that superficially looks like microcracking. A few actual surface microcracks are also noted. 8(a) 20X; 8(b) 1000X and 8(c) 3000X.

Figure 9. Compact tension specimen of Lexan neat resin (without copel rubber), coated with Au/Pd, and then loaded in-situ in the SEM. The same "wing shaped" damage zone noted in Figure 8 is seen here. However, the primary difference is the appearance of dense microcracking which is clearly in the film rather than the substrate. 9(a) 200X; 9(b) 1000X; 9(c) 2000X; 9(d) 3000X; 9(e) 1000X; 9(f) 1000X.

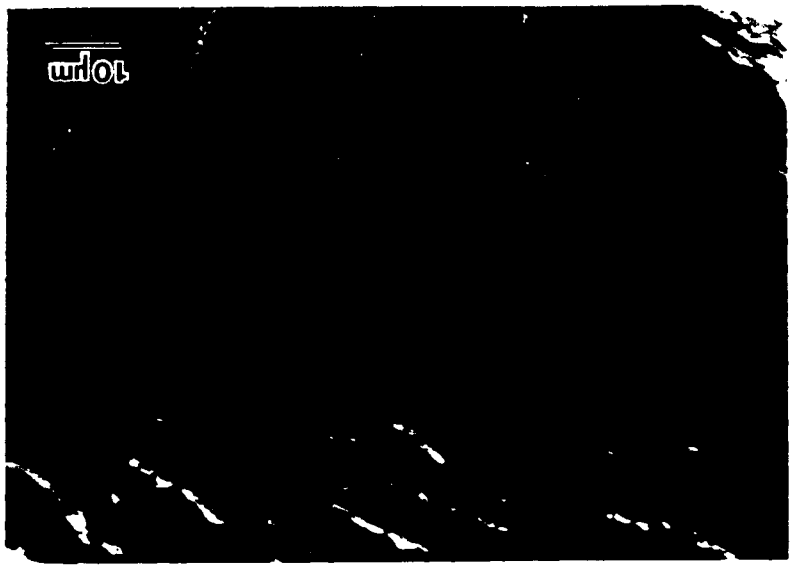

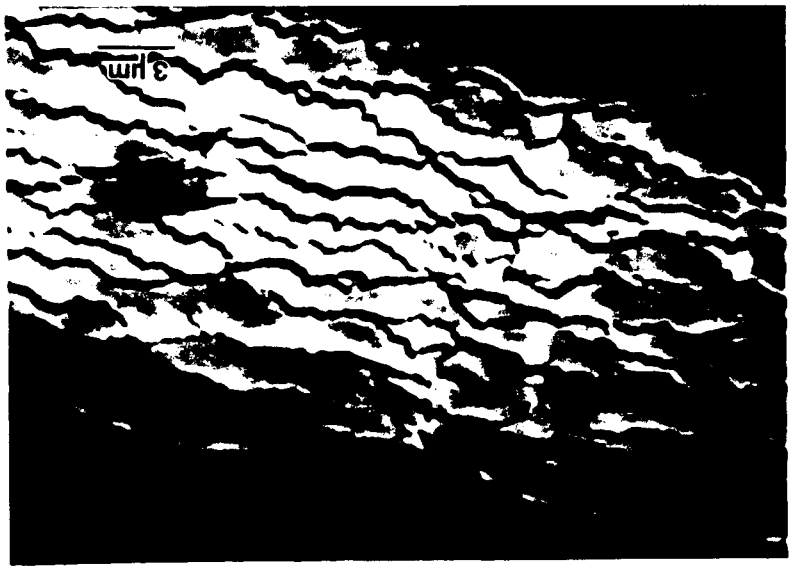

Figure 9(d), 9(e) and 9(f). (caption on previous page)

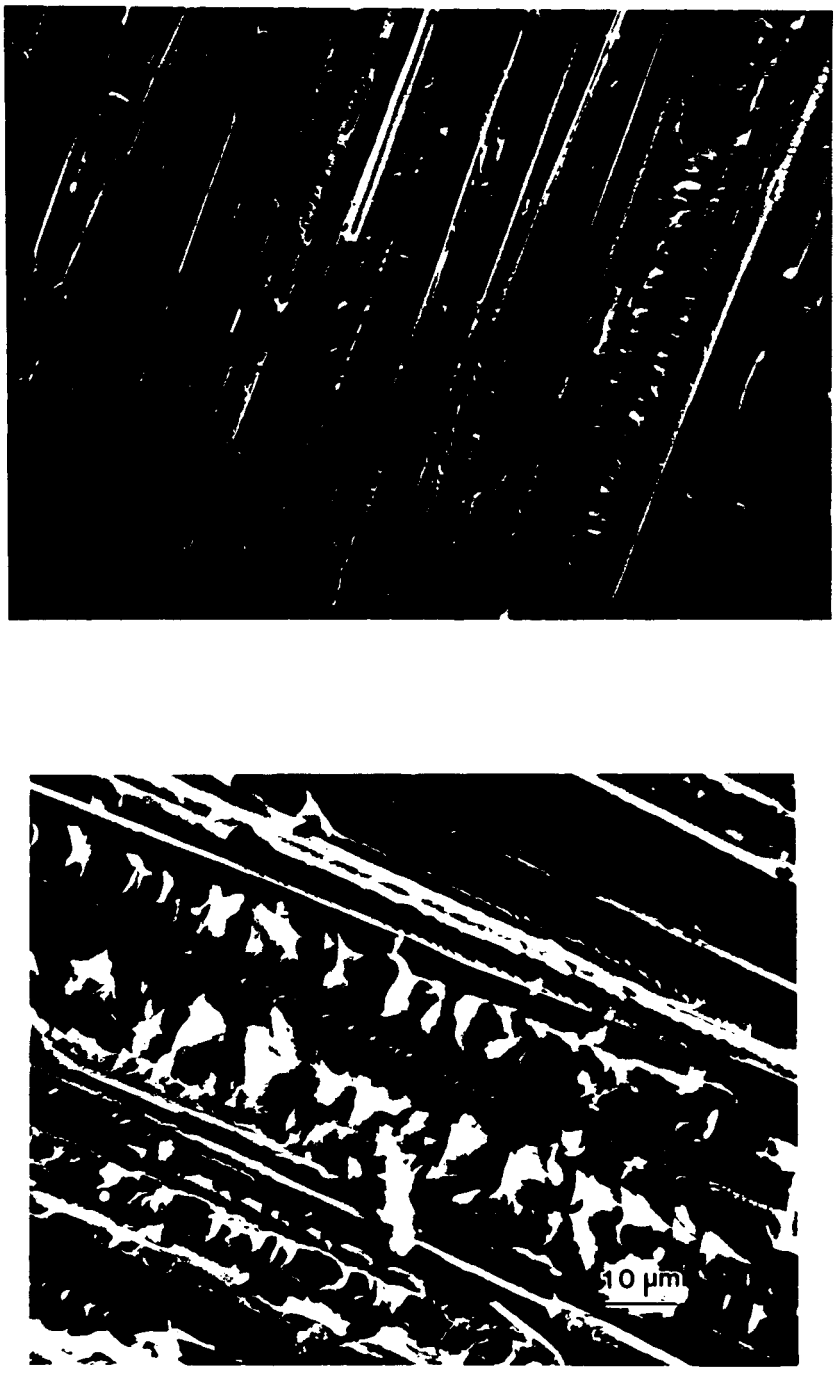

Figure 10. AS4-W6/Lexan Mode I delamination fracture surface; observed post-mortem in the SEM. 10(a) 200X; 10(b) 1000X; 10(c) 3000X; 10(d) 7000X.

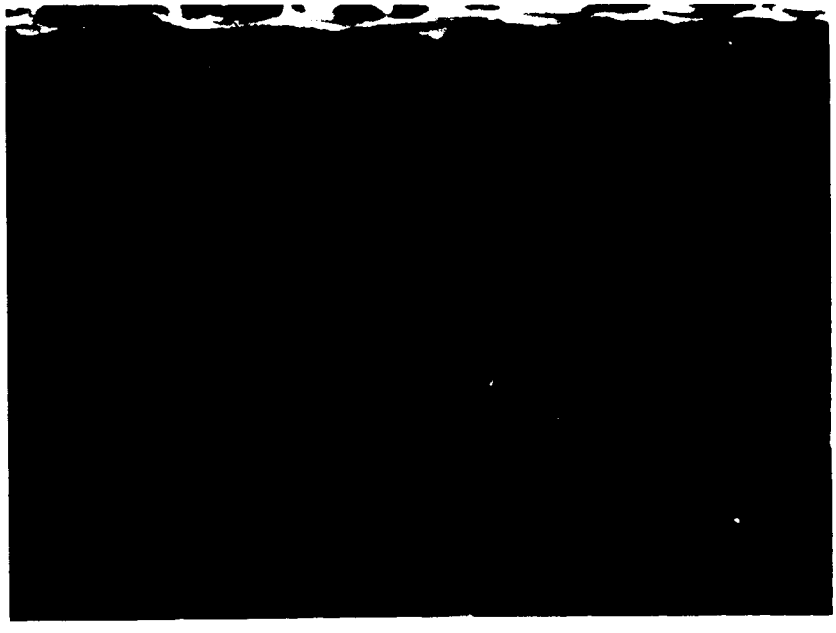

Figure 10(c) and 10(d). (caption on previous page).

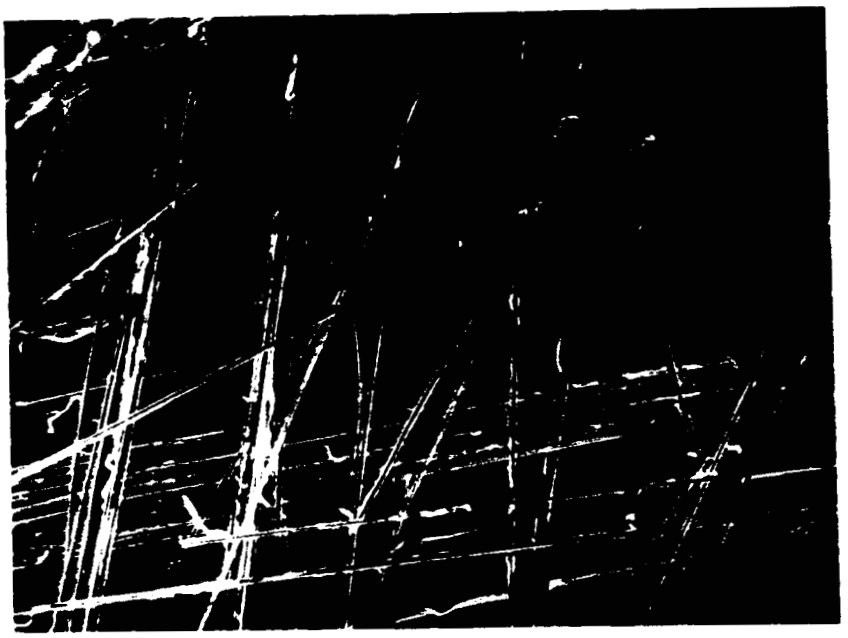

Figure 11. AS4-W6/Lexan with 10% copel rubber. Post-morten fractography of fracture surface after mode I delamination. The many loose fibers and the high magnification examination of these fibers indicates very poor interfacial bonding. 11(a) 100X ; 11(b) 4500X

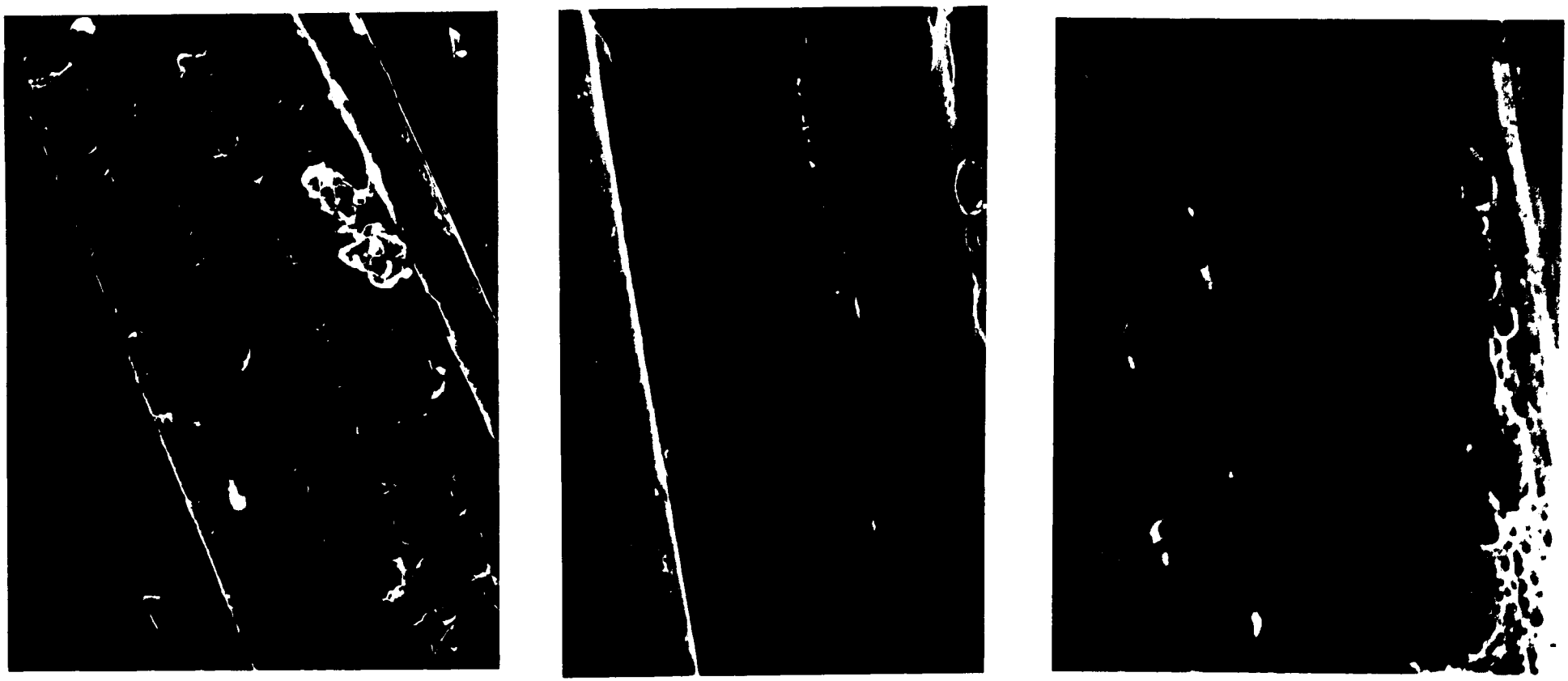

Figure12. AS4-W6/Lexan with 10% copel rubber. Post-mortem fractography of fracture surface after mode I delamination. Poor interfacial adhesion is indicated. A high magnification closeup of the interfacial failure (12c) indicates copel rubber segregation to the interface. Figures 12(d) and 12(e) show large scale deformation in a resin rich region of the composite. 12(a) 1000X; 12(b) 3000X; 12(c) 10,000X; 12(d) 3000X; and 12(e) 4500X.

Figure 12(d) and 12(e). Caption on previous page.

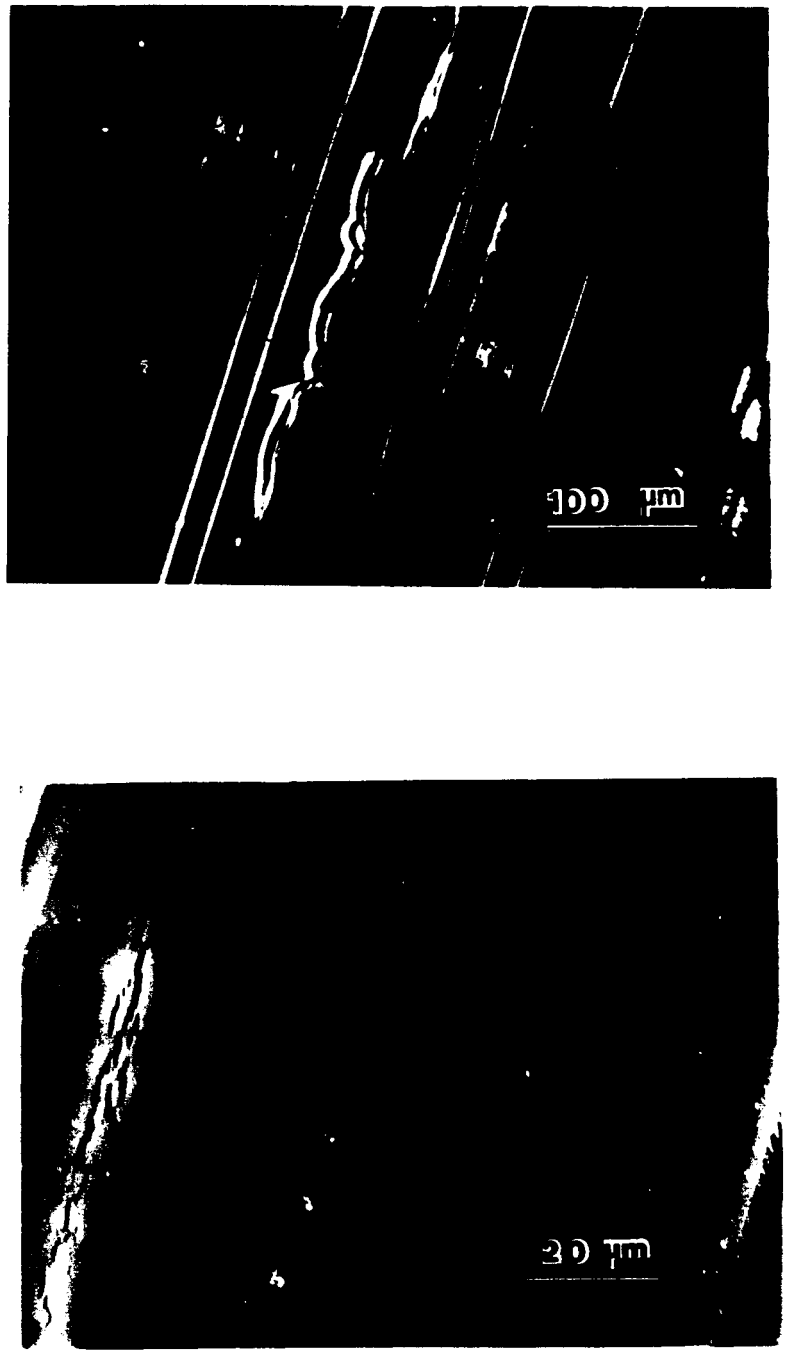

Figure 13. Mode I delamination fracture of AS4-W6/Lexan fractured in-situ in the SEM. Macrocrack and microcracks observed are considered to be real substrate cracks, not just coating cracks. 13(a) 300X; 13(b) 1100X; 13(c) 3000X; and 13(d) 3000X.

Figure 13(d) and 13(e). (caption on previous page)

Figure 14. Mode I delamination fracture of AS4-W6/Lexan with 10% copel rubber fractured in-situ in SEM. Macrocrack and coarse microcracks are considered to be substrate cracks in resin whereas very fine network of micro-cracks are interpreted to be film microcracks. 14(a) 300X; 14(b) 1000X; 14(c) 3000X.

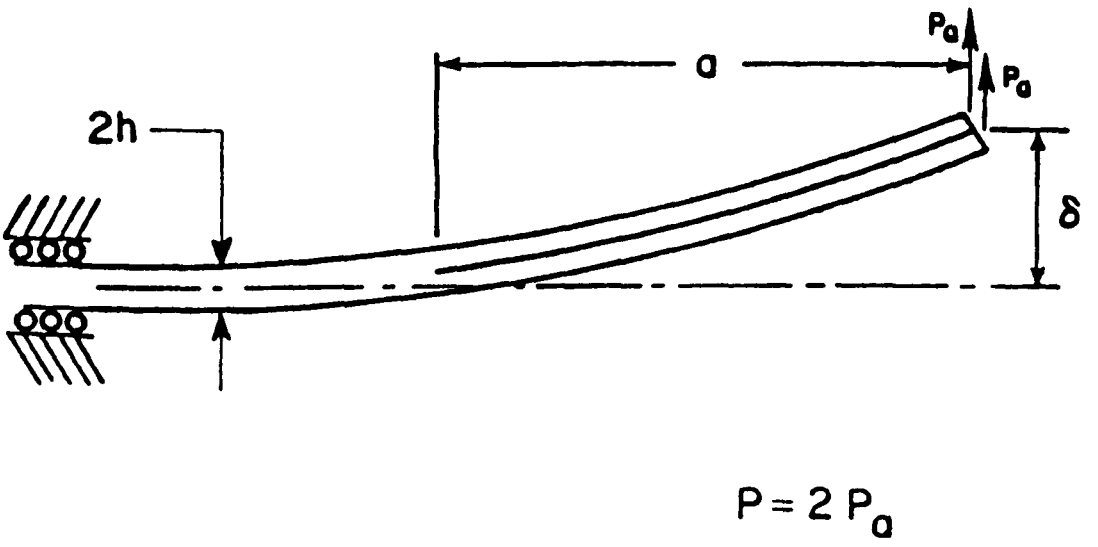

Figure 15 ELS test configuration and associated parameters.

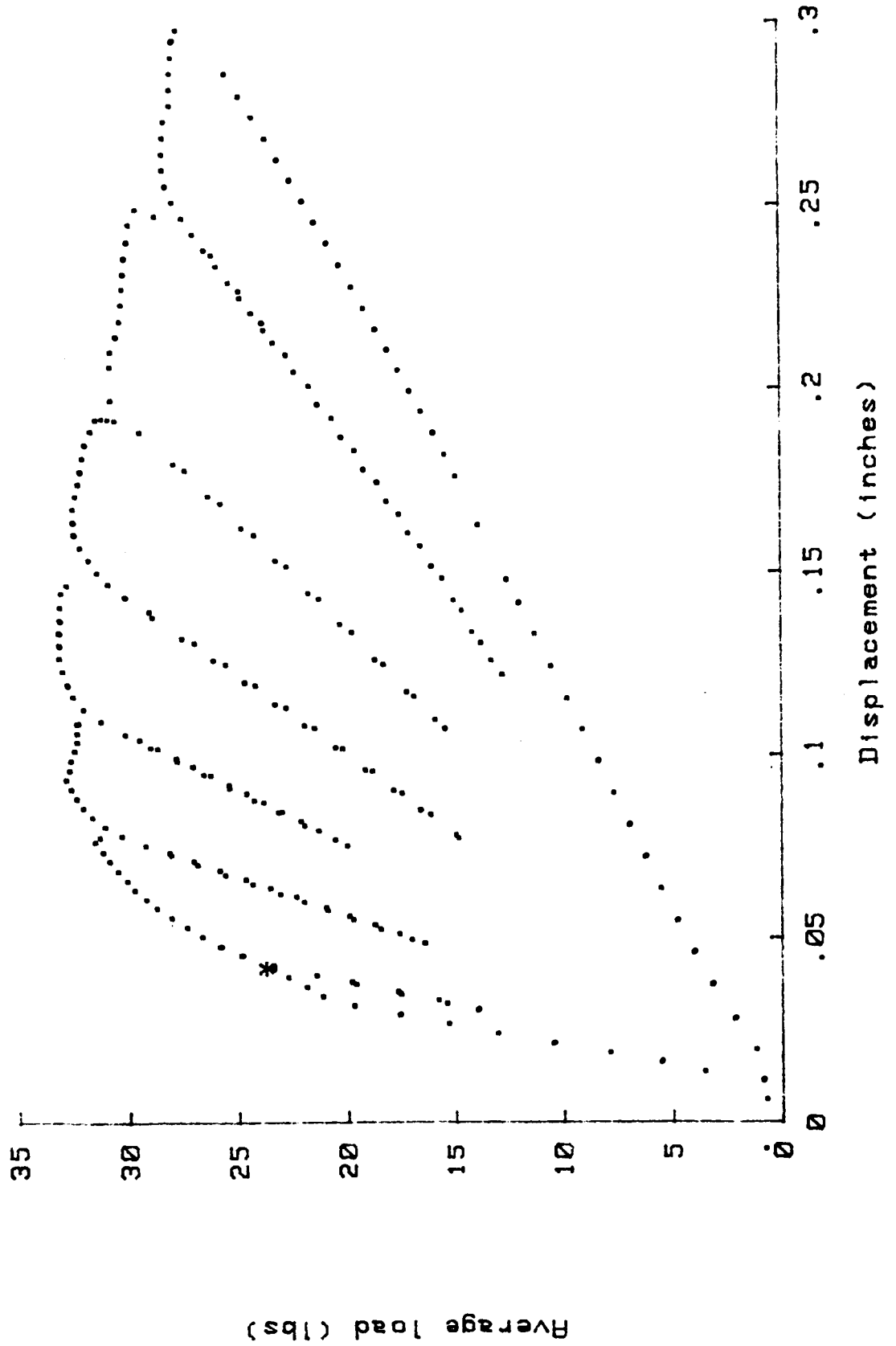
AS4-W6/LEXAN-10% COPEL MODE I DELAMINATION
Average load (lbs)
Displacement (inches)
0
5
10
15
20
25
30
35
.05
.1
.15
.2
.25
.3

FIGURE 16 -

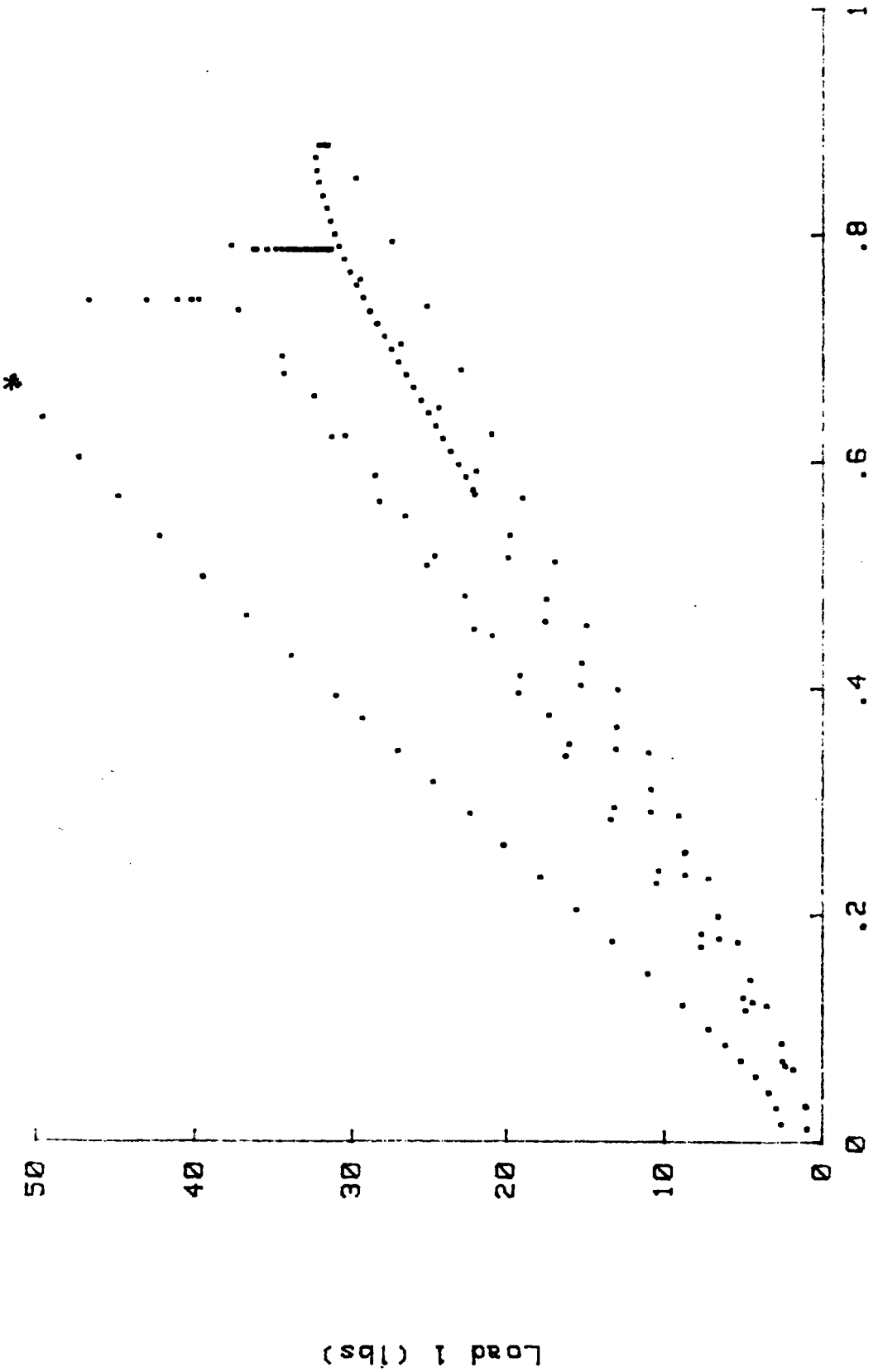
AS4-W6/LEXAN-10% COPEL MODE II DELAMINATION
Load 1 (lbs)
50
40
30
20
10
0
0
.2
.4
.6
.8
1
Displacement (inches)

FIGURE 17 -

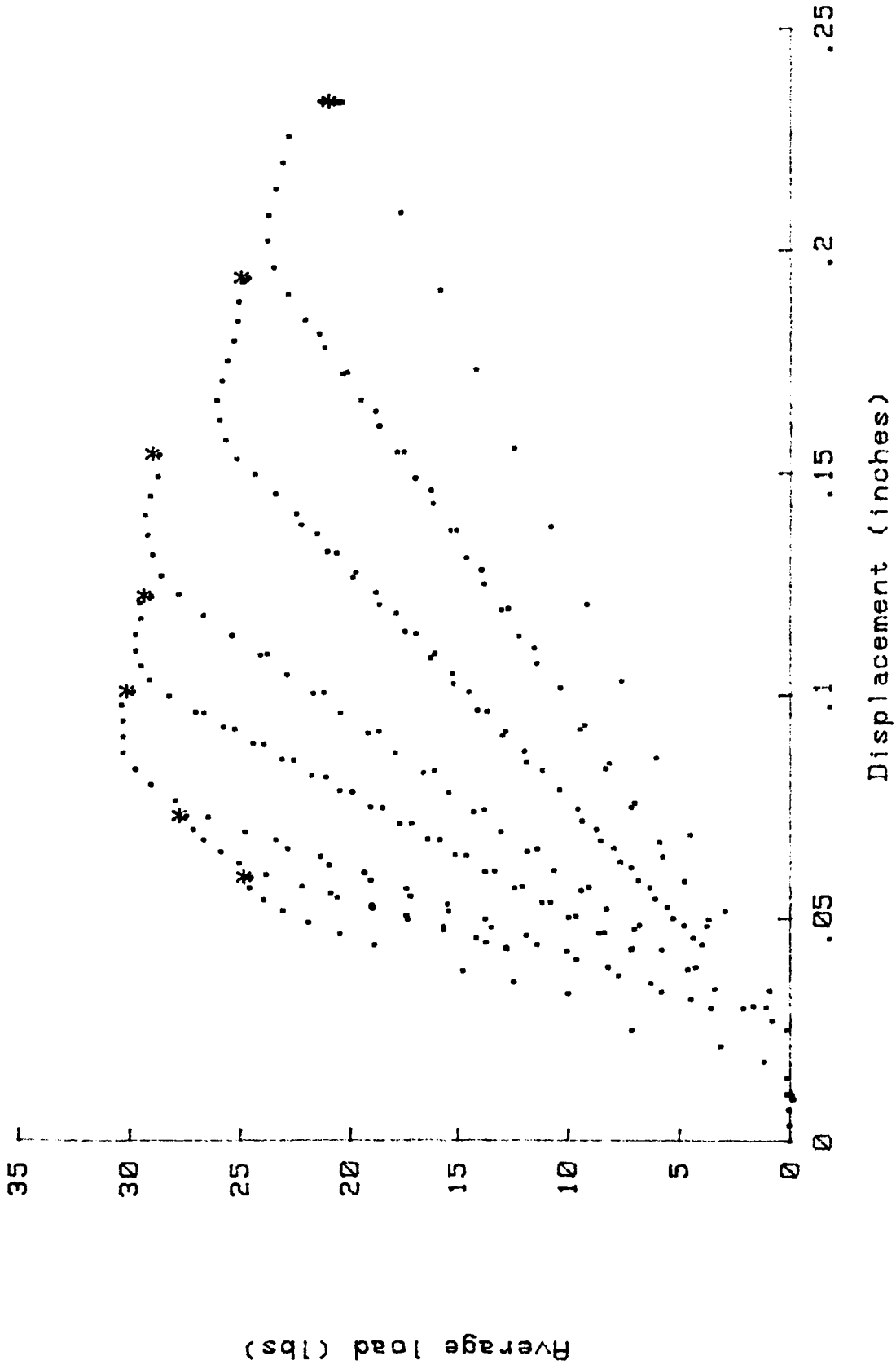
AS4-W6/LEXAN MODE I DELAMINATION
Average load (lbs)
35
30
25
20
15
10
5
0
0
.05
.1
.15
.2
.25
Displacement (inches)

FIGURE 18 -

FIGURE 19 - AS4-W6/LEXAN MODE II DELAMINATION

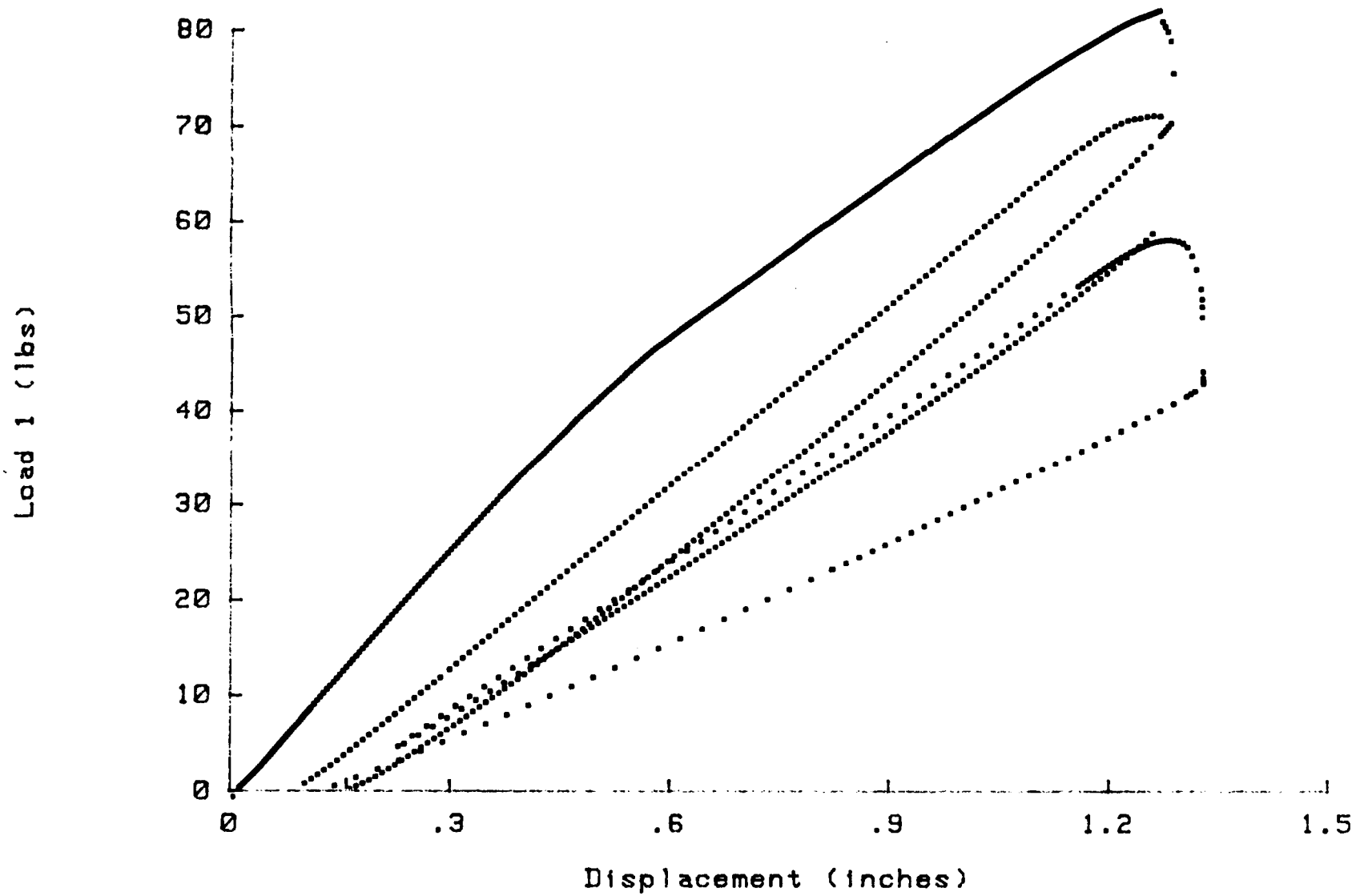

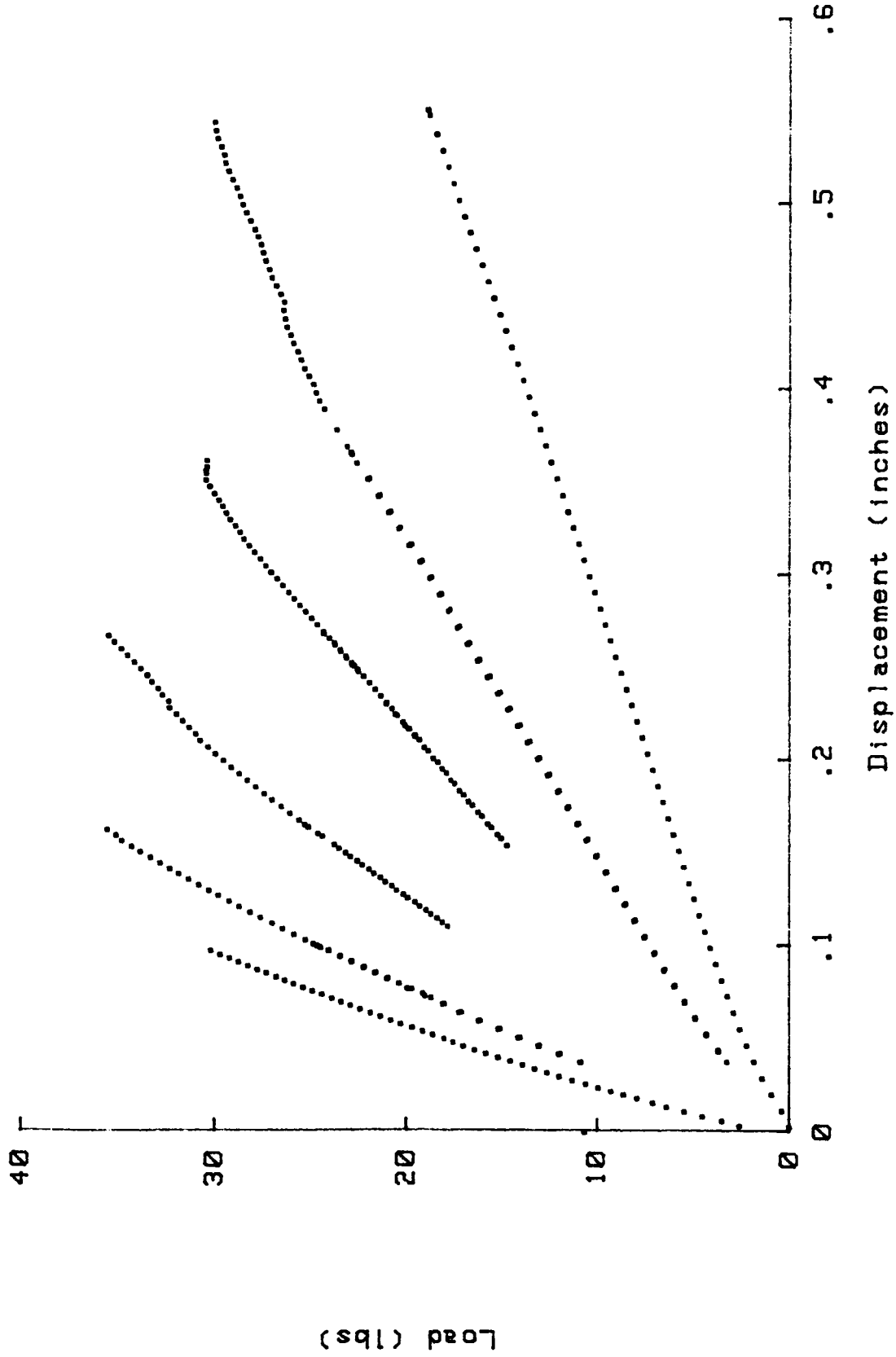
AS4/PEEK APC-2 MODE I DELAMINATION
Load (lbs)
40
30
20
10
0
0
.1
.2
.3
.4
.5
.6
Displacement (inches)

FIGURE 20 -

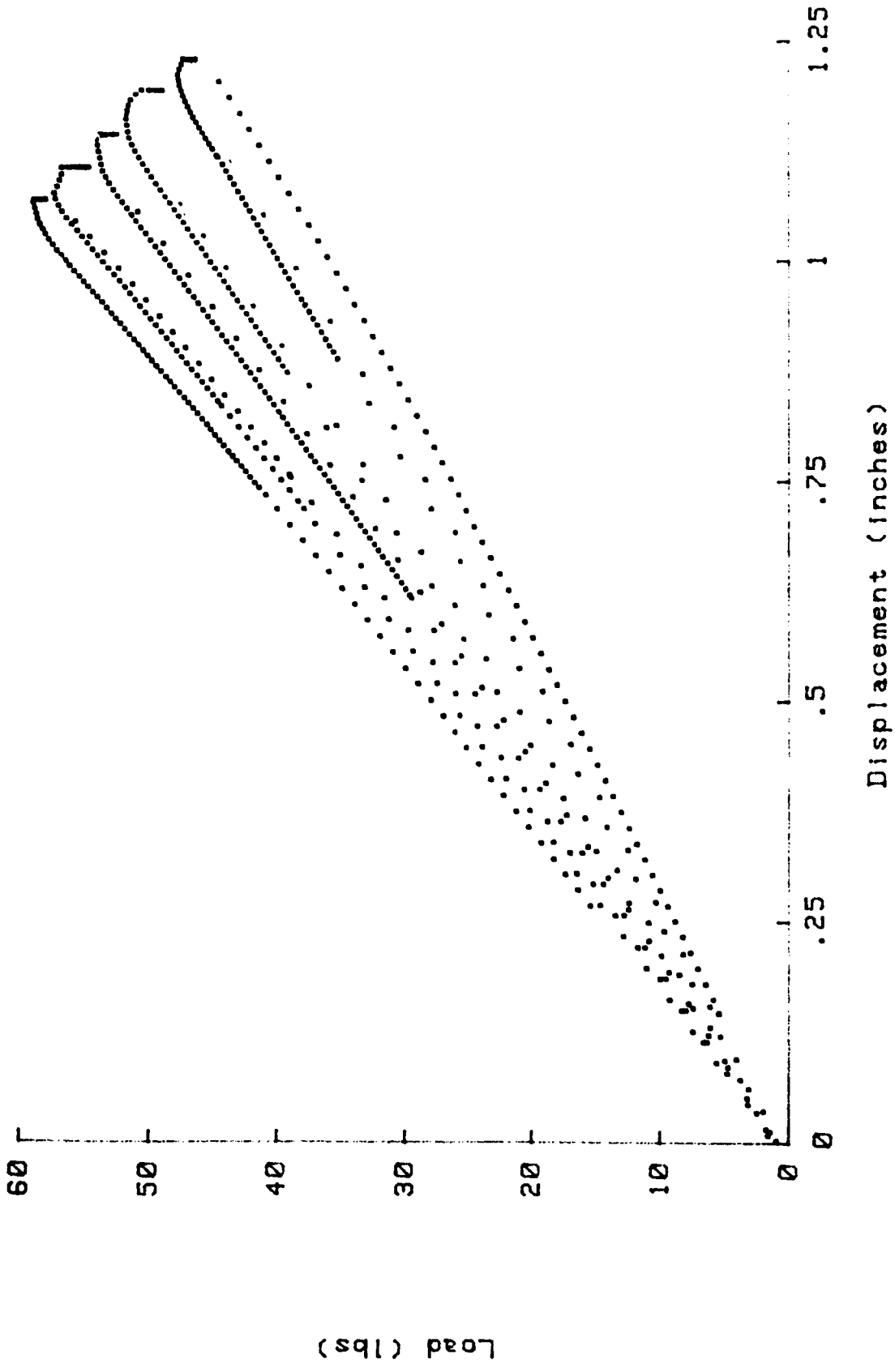
AS4/PEEK APC-2 MODE II DELAMINATION
Load (lbs)
60
50
40
30
20
10
0
0
.25
.5
.75
1
1.25
Displacement (inches)

FIGURE 21 -

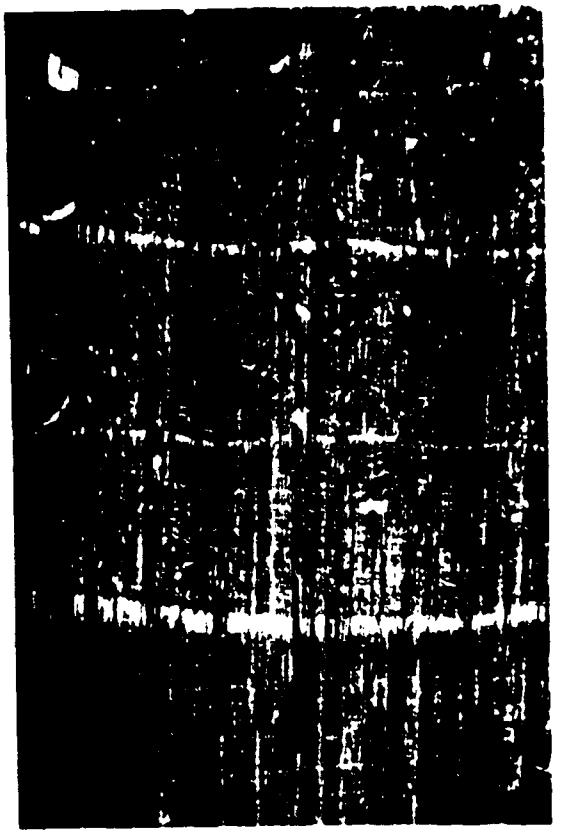

Figure 22. Macrofractographic view of Mode I delamination fracture surface for PEEK composite showing the duplex appearance that results from stable and unstable delamination crack growth. 3X

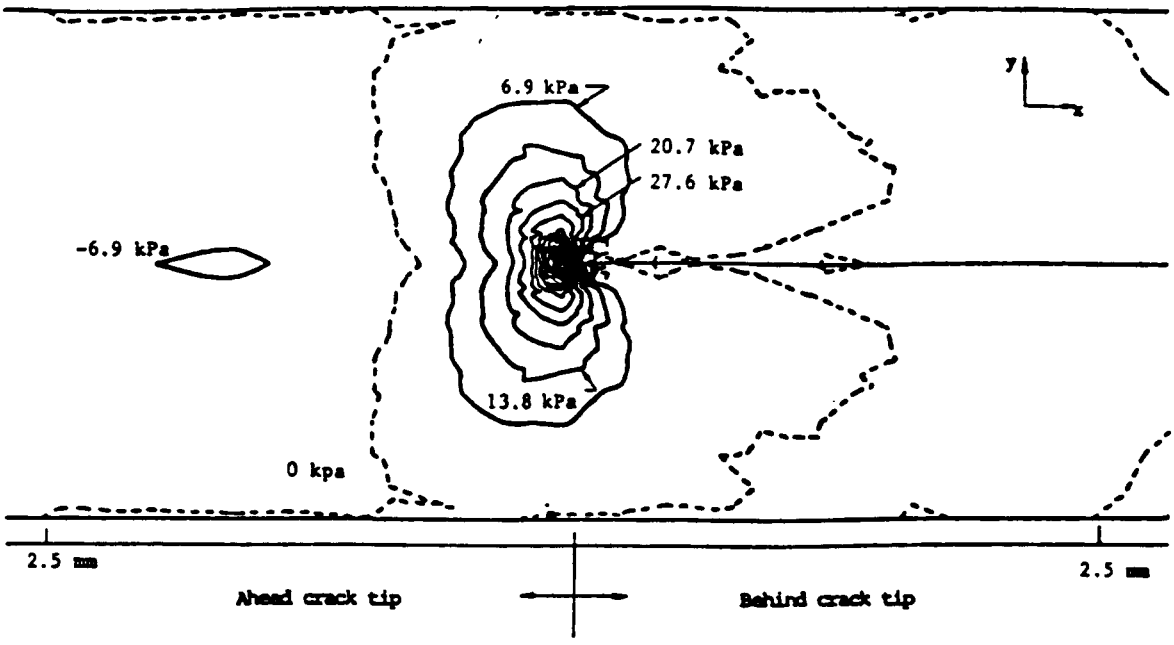

(a)

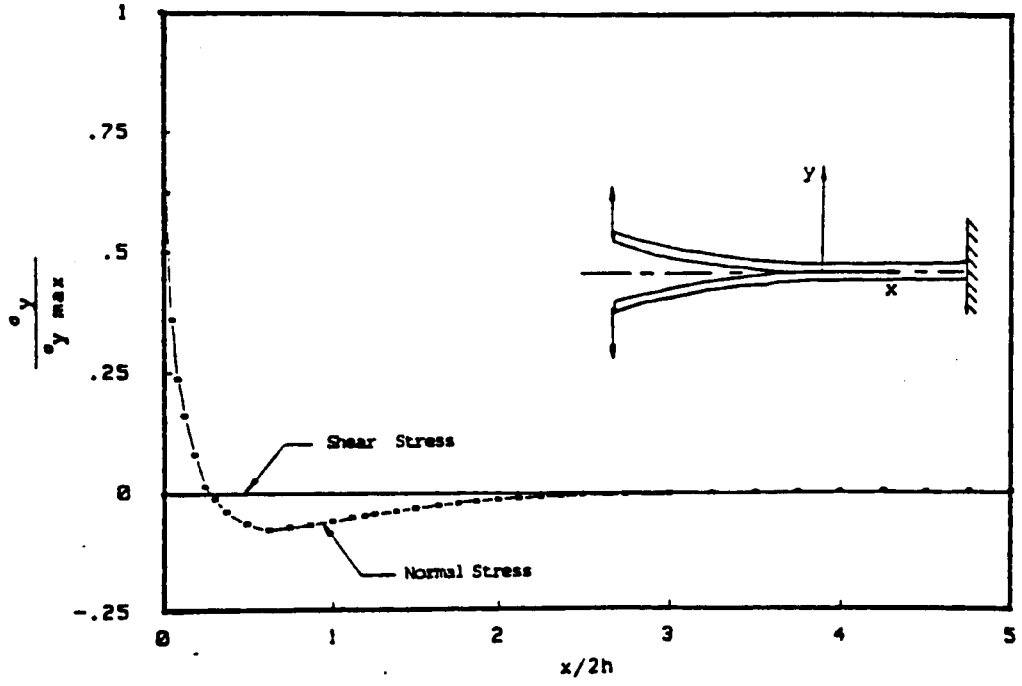

(b)

Figure 23 (a) σ_y stress contour plot and (b) stress field ahead of crack tip, of split laminate beam tested under mode I conditions.

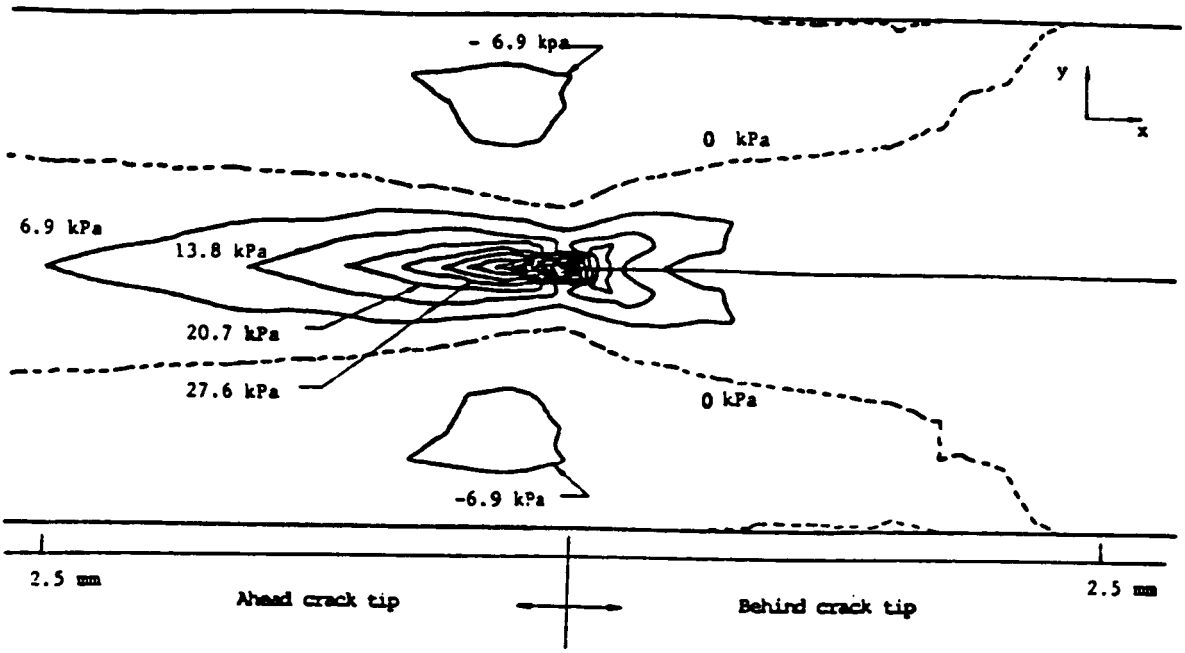

(a)

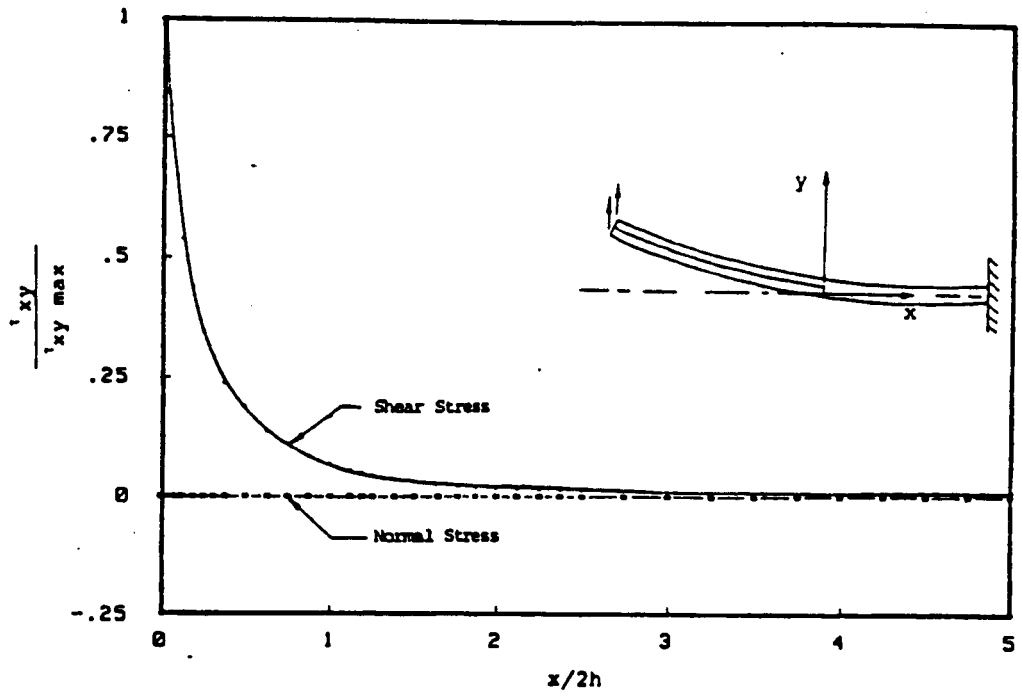

(b)

Figure 24 (a) τ_{xy} stress contour plot and (b) stress field ahead of crack tip, of split laminate beam tested under mode II conditions.

Figure 25 Damage zone under Mode I delamination of AS4/3501-6 graphite epoxy composite (90 μm long, and 10-15 μm wide) 3000X

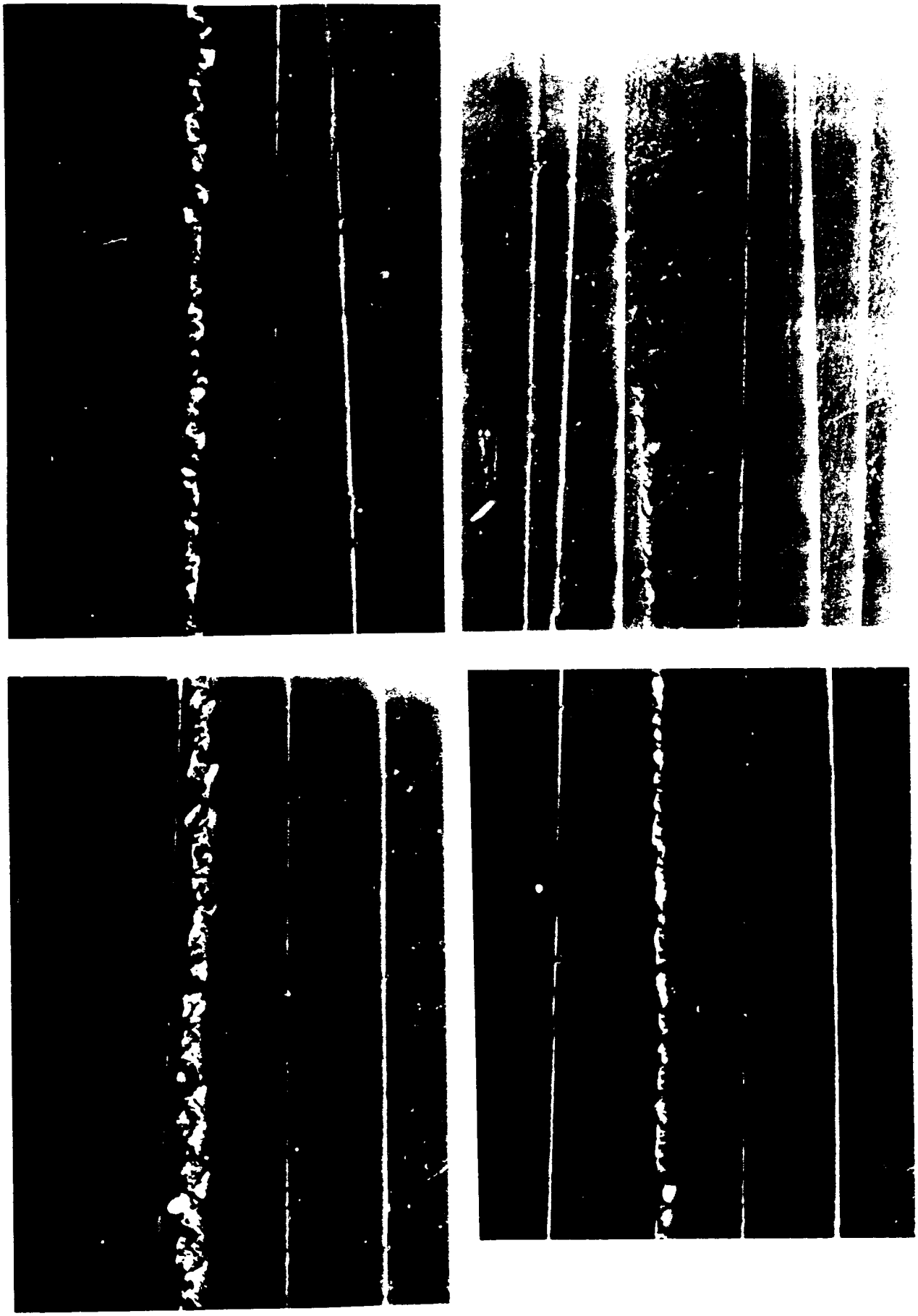

Figure 26 Mode II delamination zone in AS4/3501-6 graphite/epoxy (270 μm long, <5 μm wide). 2000X

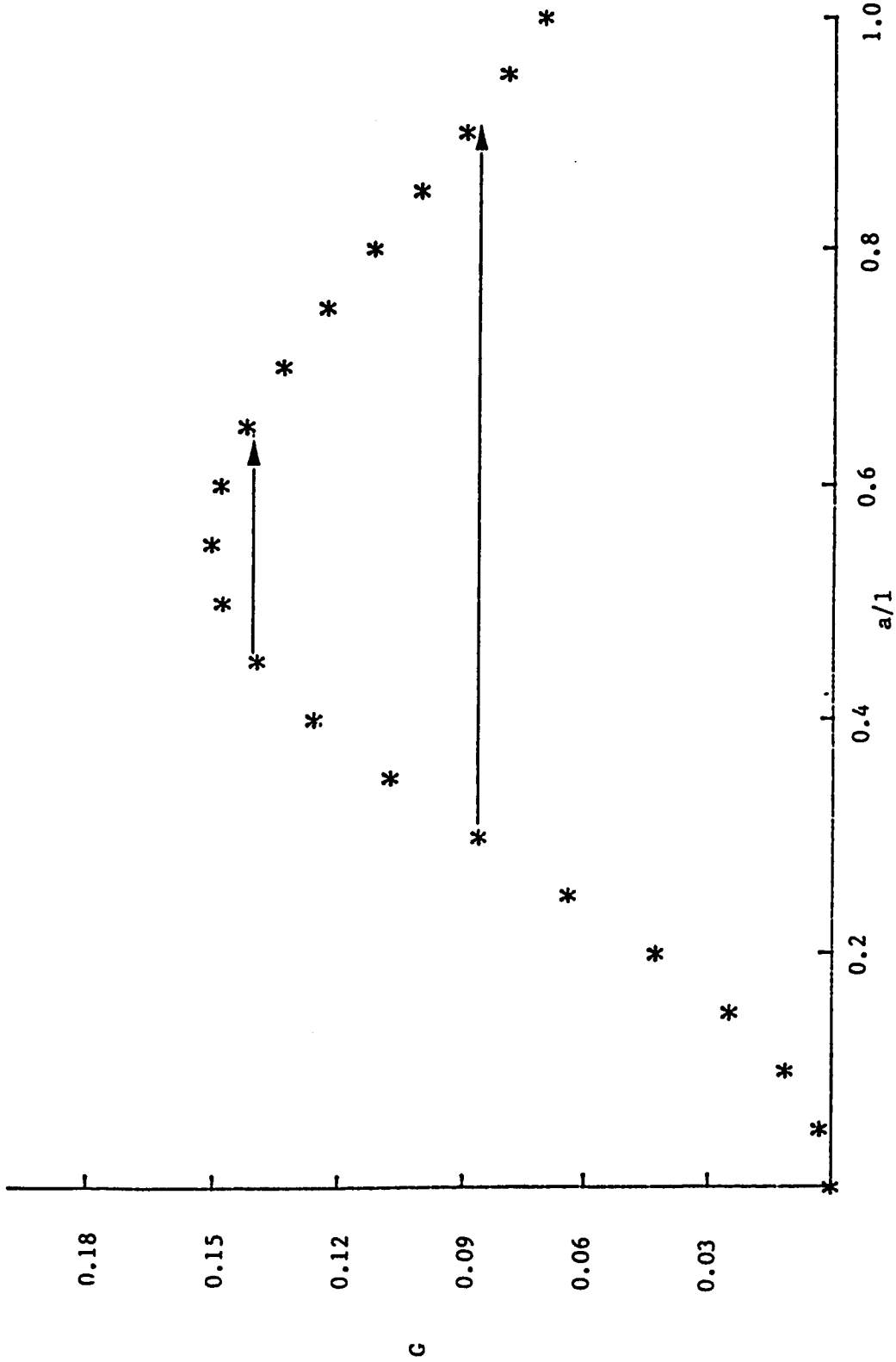

Fig. 27 Plot of G vs. a/l for an end-loaded flexure test showing extent of unstable crack growth for two initial a/l values (0.3 and 0.45). Note G is a dimensionless quantity.

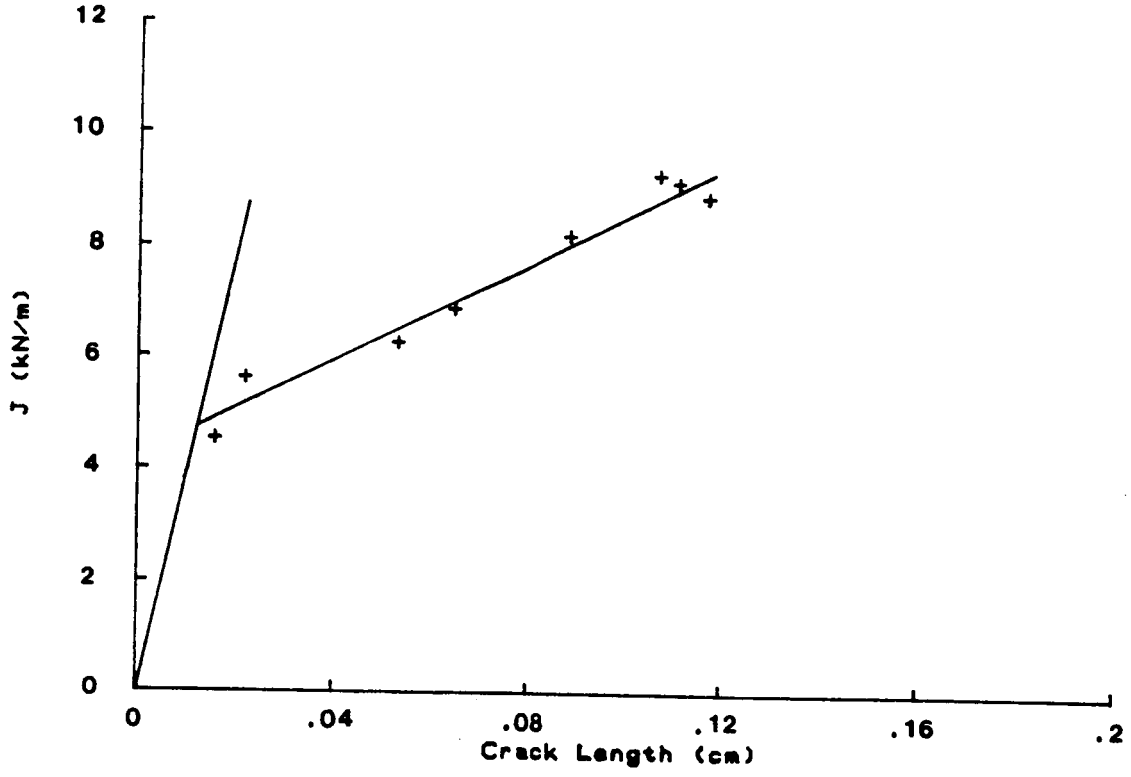

Figure 28 J-R Curve for Non-annealed Razor Notched PE

APPENDIX I

A COMPARISON OF THE CRACK TIP DAMAGE ZONE FOR FRACTURE OF HEXCEL F185 NEAT RESIN AND T6T145/F185 COMPOSITE

E. A. Chakachery and W. L. Bradley

Texas A&M University

College Station, TX 77445

Presented at the ACS International Symposium

on Non-Linear Deformation, Fatigue and Fracture

of Polymeric Materials

ABSTRACT

A Comparison of the Crack Tip Damage Zone for Fracture of Hexcel F185 Neat Resin and T6T145/F185 Composite, E. A. Chakachery and W. L. Bradley, Texas A&M University, College Station, 77843. Hexcel F185 neat resin and T6T145/F185 graphite fibre reinforced composite were subjected to Mode I loading in the compact tension geometry (fibres parallel to the crack) and the energy per unit area of crack extension, J_{IC}, determined to be 8100 and 1600 J/m^2 respectively. In-situ fracture studies in the SEM on a CT-type specimen of F185 showed extensive micorcracking in a damge zone ahead of the crack tip, which was similar to the microcracking observed in the whitened area ahead of the crack tip in the macroscopic CT specimens. A simple calculation using a rule of mixtures approach suggests that the diminished size of the damage zone and the presence of rigid fibres in the damage zone in the composite are not a sufficient explanation to account for the significantly lower toughness of the composite compared to the neat resin. From this it may be inferred that the strain to failure locally in the damage zone ahead of the crack in the composite may also be lower than that which can be tolerated in the neat resin. Evidence for this idea comes from the observation that microcrack coalescence seems to occur preferentially at the fibre/resin interface.

INTRODUCTION

Delamination in graphite fibre reinforced resin composites is well known to limit the extensive use of these materials in some structural applications. Much effort has been directed in the past decade towards improving the delamination fracture toughness of graphite/epoxy composites (1-10). Since the delamination crack propagates through the interlaminar resin rich region, the emphasis has been on obtaining epoxy resins with improved fracture toughness. The addition of elastometric modifiers was shown (1-6) to dramatically increase the fracture toughness, G_{Ic}, of the matrix resin, but resulted only in a modest increase in the delamination fracture toughness of the composite (7,8). This was shown (8-10) to be primarily due to the reduced volume of resin deformation in the damage zone ahead of the delamination crack tip since the fibres act as rigid fillers in the ductile matrix. Evidence in support of this conclusion was obtained (9,10) from the observation that a decrease in the fibre volume fraction resulted in an increase in the delamination fracture toughness. The current investigation was undertaken to attempt to correlate the delamination fracture toughness of the composite with the fracture toughness of the neat resin. The determination of the fracture processes occurring in the vicinity of the crack tip in both the composite and the neat resin was a necessary first step. If these events are nominally the same, then there may be a relationship between neat resin toughness and delamination toughness.

To study the relationship between neat resin fracture toughness

and composite delamination fracture toughness, in-situ observations of each fracture process have been made in the scanning electron microscope. These observations have been correlated with macroscopic measurements of a composite made from this neat resin. A simple model has been proposed to relate the microscopic observations of the fracture processes to the observed macroscopic measurements of fracture toughness.

The resin system selected for this study was the F185 formulation commercially available from Hexcel Corp. It is a relatively ductile epoxy (9% elongation in a 2.5 cm gage section) with a reported fracture toughness of 6000 J/m^2 (7,11). The resin is primarily a diglycidyl ether of bisphenol A, (DGEBA), modified by the addition of 8.1 wt% of liquid CTBN (Hycar® 1300 x 13), a carboxyl terminated copolymer of butadiene and acrylonitrile. It is further toughened by the addition of 5.4 wt% of Hycar® 1472, a pre-reacted solid elastomer in a bimodal particle size distribution of nominally 2 μm and 8 μm diameters. The liquid CTBN undergoes partial phase separation into particles varying from 0.1 m to 10 m in size. The portion that does not phase separate out before gelation of the epoxy remains in solution in the epoxy matrix and has a plasticizing effect on the resin (3,4), thus lowering the yield strength of the epoxy matrix. The phase separated CTBN undergoes dilatation and rupture by cavitation (5,6) thus reducing the triaxial state of stress in the vicinity of the particle. This has the effect of locally increasing the shear stress and promoting deformation through the formation of shear bands (5,6).

EXPERIMENTAL PROCEDURES

Materials and Specimen Preparation

The F185 neat resin and the T6T/145/F185 graphite/epoxy composite used were both supplied by Hexcel Corporation. Plates, 1.25 cm, 0.5 cm, and 0.2 cm thick, of F185 were received as cast, and were machined according to ASTM E 813-81 to obtain standard 1T compact tension (CT) specimens, but with a thickness of 1.25 cm. The T6T145/F185 composite was obtained both as preimpregnated tape (25 cm wide) and as undirectional plates, 90 plies thick (A) and 24 plies thick (B). Compact tension specimens were machined from plate A such that the fibers and the laminate lay-up axis were transverse to the load line, with the direction of crack propagation parallel to the fibres. As with the F185 resin these were standard 1T compact tension specimens with a thickness of 1.25 cm. Plate B contained a teflon strip (2.5 cm wide, running perpendicular to the fibre direction) between the twelfth and thirteenth plies. This created a region of debond which acted as an initial delamination crack. Two undirecitonal plates, sixteen plies (C) and twelve plies thick (D), were laid up from the preimpregnated tape with mid-plane teflon inserts (as in plate B), and cured according to the schedule described in the specification sheet supplied by Hexcel Corporation. Double cantilever beam (DCB) specimens (2.5 cm wide and 25 cm long) were machined from plates B and C such that the fibre direction was parallel to the specimen length. Tabs which allowed for free rotation were bonded to the DCB specimens at the end with the initial delamination crack.

Miniature DCB specimens of the composite (3.8 cm long and 0.7 cm wide) were cut from plate D and minature CT-type specimens of the neat resin (4 cm long, 2.8 cm wide and 0.2 cm thick) were also machined for in-situ studies. These were ground, polished (0.25 μm), cleaned ultrasonically and coated with a Au/Pd alloy (~150 A) prior to observation in the scanning electron microscope.

Specimen Testing

All macroscopic testing of DCB and CT specimens were performed on a Materials Test System (MTS) servo-hydraulic machine in displacement control under quasi-static loading conditions (4×10^{-5} to 7×10^{-5} cm/sec) at room temperature. Load-displacement records were obtained directly from the MTS strip chart recorder and were also digitized simultaneously via a Hewlett-Packard HP 3497A Data Acquisition Unit and stored through a HP 9816 desk-top computer. All CT specimens were machined with a chevron notch and were pre-cracked in fatigue until the crack front was out of the chevron. Fatigue load limits were determined as per ASTM E 399-81 for the composite and ASTM 813-81 for the F185 resin. Post-mortem fractography was performed on a JEOL JSM-25 scanning electron microscope. A JEOL JSM-35CF scanning electron microscope equipped with a JEOL 35-TS2 tensile stage was used for the fracture studies in-situ in the SEM. Photomicrographic stills and real-time videotapes were obtained of the fracture processes.

RESULTS, ANALYSIS AND DISCUSSION

Macroscopic Fracture Toughness Measurements

The load-displacement results for the delamination tests were analyzed using a relationship derived from linear beam theory by Devitt et al (12), namely,

$$G = \frac{P^2 L^2}{BEI} \qquad (1)$$

where P is the load, L is the crack length, B is the width, E is the tensile modulus and I is the rotational moment of inertia for each half of the split laminate. The ratio of load line displacement to crack length remained well below the limit of 0.6 for linear beam theory to be applicable (12). The crack length was measured visually at the surface at approximately fifteen discrete points and the loads and displacements recorded at these same points. Critical energy release rates could then be calculated for each point. The calculated G_{Ic} values remained essentially constant for various crack lengths. An average of the calculated values after the transient was found to be 1900 J/m^2 .

The 1T compact tension specimens of F185 was tested in displacement control with multiple, partial unloading to allow determination of the crack extension by the compliance method. The load-displacement record was quite nonlinear (Fig. 1), necessitating a J-integral analysis according to ASTM E813-81. A well defined J-R curve was obtained from which a J_{Ic} value of 8100 J/m^2 was determined.

This is considerably higher than the value of 6000 J/m^2 reported by the manufacturer (11). This difference may be due to our use of fatigue precracking rather than razor notching or due to our use of a nonlinear rather than linear analysis. If we use the linear elastic analysis in ASTM E399-81,we obtain a K_Q value of 2700 J/m^2 from the 5% secant offset value of P_Q. However, Pmax is much greater than 1.1 P_Q, and the specimen thickness is less than that required by ASTM-E399 for K_Q to be equal to K_{Ic}. Thus, the linear elastic analysis is invalid for our specimen size. If we use Pmax and the actual crack length at Pmax in a LEFM calculation, we obtain a "K_{Ic}" which has an equivalent G_{Ic} of 6300 J/m^2 which is similar to the 6000 J/m^2 obtained by Bascom (2) using a similar approach. We believe that the value of 8100 J/m^2 obtained in this work using fatigue precracked specimens and a J-integral analysis is a more meaningful measure of the fracture toughness of the F185 resin.

A J-integral approach was also used to analyze the data obtained in the CT specimens of the composite. The J_{Ic} for transverse crack growth thus obtained was 1600 J/m^2 which compares very well with recent results by Bascom (13). The macroscopic test may be summarized as follows: the neat resin fracture toughness was 8100 J/m^2 whereas the delamination and transverse cracking in the composite gave toughness values of 1900 J/m^2 and 1600 J/m^2 respectively. Thus, crack growth in the composite parallel to the fibre direction is much easier than crack growth in the neat resin.

In-Situ and Post Mortem Fracture Observations in SEM

Fracture studies conducted in the scanning electron microscope on

the F185 neat resin indicate that the zone ahead of the crack tip undergoes extensive microcracking (Fig. 2). There has been some recent controversy as to whether these are actually microcracks in the resin or microcracks in the 150A thick gold-palladium coating applied to the specimens to minimize charging. To try to verify that these are actual microcracks in the material, we have recently polished two sides of an AS4/3501-6 graphite/epoxy composite, coated one side with a 150A thick layer of gold-palladium in the usual way, delaminated the specimen in the SEM, removed the specimen with the wedge in tact to avoid viscoelastic recovery and closure of the microcracks, and then coated the other side with gold-palladium in the usual way, and then examined it in the SEM with the wedge still in tact. The results of this exercise are presented in Figures 3(a) and 3(b). The microcrack morphology on the side coated and then deformed is essentially indistinguishable from the microcrack morphology seen on the side deformed and then coated. Thus, we believe that the Au/Pd coating is not responsible for the microcracking seen on the surface of our specimens.

The microcracked region ahead of the crack tip of the F185 neat resin (Fig. 2) extends 60-70 μm above and below the crack tip and is shaped somewhat like a kidney bean. Crack propagation under fixed grip conditions occurred in a discontinuous manner via a time-dependent coalescing of the microcracks ahead of a blunted crack tip. With each successive extension, crack advance of 120-150 μm was observed, resulting in a very sharp crack tip with relatively few microcracks ahead of it. The applied crack opening displacement was

then increased essentially instantaneously, and with this increase, the microcrack density ahead of the crack tip would gradually increase with time, accompanied by crack tip blunting at the formerly sharp crack tip. Again, a critical density of microcracks (or crack tip strain) is reached and crack extension occurs by microcrack coalescence as before. Evidence of this process is seen in the post-mortem fractographic examination as relatively flat regions of crack extension, separated by the small lips which probably arise from crack tip blunting, preceding the next crack extension (Fig. 4). This appearance is typical over the whole fracture surface, indicating that the phenomena observed at the surface is typical of the bulk fracture behavior.

If crack extension does indeed occur by microcrack coalescence, then the relatively flat regions between lips seen in Figure 4(a) and (b) should be found on examination at higher magnification to be composed of many small facets with ledges between them. This is exactly what is observed at 10,000X magnification, as shown in Figure 4(c). It is worth noting that even at this very high magnification that the individual facets do not seem to have fractured by a brittle cleavage. The surface is relatively textured, with cavitation presumably at the rubber particle additions, which suggests that the microcracking is a result of heterogeneous nucleation and growth by processes which require some local deformation. Thus, the microcracking may be a result of heterogeneities in the resin which facilitate crack nucleation and growth.

If the microcracks were just a result of coating cracking, the explanation would still be much the same except that the microcracking

would correspond to some threshold level of resin strain with the microcrack coalescence corresponding to some critical strain to failure in the resin. Thus, though we believe that the microcracks are in the resin rather than in the coating, the inference concerning the size of the deformation/damage zone ahead of the crack tip can be made equally well in either case. It should also be noted that microcracking and deformation have the same beneficial effect of redistributing the load away from the crack tip and lowering the local stresses at the crack tip. Thus, from a physical point of view, either process enhances toughness.

In-situ delamination studies on T6T145/F185 composite show that the resin microcracks quite extensively in the vicinity of the crack tip. The microcracking extends from the interlaminar region and into the ply about 50 μm above and below the crack (Fig. 5). Here, as in the resin, the crack propagates by microcrack coalescence and in the same discontinuous manner. At each stage, however, the crack tip blunting is apparently less than in the F185 resin and the discontinuous extension varies from 40-100 μm. The coalescence of microcracks occurs predominantly at the fibre resin interface. Thus it appears that the presence of the fibres prevents the development of the full resin toughness from being realized due to premature microcrack coalesence at the fibre resin interface.

The presence of the rigid fibres also restricts the height above and below the delamination plane over which deformation and microcracking occurs (100 μm in the composite, compared to 130 μm in the resin). However, the region of microcracking ahead of the crack

tip is actually increased from 25 μm in the resin to about 50 μm in the composite.

The fracture surface of the delaminated specimens showed evidence of cavitation, voiding and microcracking(Fig. 6). The resin region of the composite delamination fracture surface shows more coarse cavitation than in the neat F185 resin fracture surface, where voids were relatively fine and more homogeneously dispersed. Furthermore, the voids seem to be more dense in the resin adjacent to the fibres (Fig. 6(a),(b). The fibre resin interface probably provides heterogeneous nucleation sites for precipitation of the CTBN and facilitates the growth of larger particles. Microcrack coalescence at the fibre resin interface results in the highly scalloped features noticeable in Figure 6(b).

A Model to Predict Delamination Toughness from Neat Resin Toughness

A first order estimate of the delamination fracture toughness may be obtained by assuming that the delamination fracture process is essentially the same as the fracture process in the neat resin, except that the fibres act as a rigid filler, reducing the volume of resin available to deform in the crack tip region. It has previously been suggested by Bradley and Cohen (8) that the energy dissipation per unit area of crack extension may be calculated by picturing a small tensile specimen ahead of the crack tip which is slowly stretched as the crack tip approaches and finally breaks as the crack tip passses(Fig. 7). The energy absorbed per unit area of crack extension would be calculated for such a model by summing the energy abosrbed per unit volume of material over the volume of the hypothetical

tensile specimen. Such a summation may be written mathematically as follows:

$$G_{Ic} = \int_{-h}^{h} \int_{0}^{\varepsilon_{ij}} \sigma_{ij} \, d\varepsilon_{ij} \, dy \qquad (2)$$

where G is the fracture toughness of the material

$2h$ is the height of the hypothetical tensile bar

σ_{ij} is a component of the stress tensor

The addition of fibers to the neat resin can perturb the energy calculation in Equation 2 in several ways. First, the extent of the deformation zone might be changed (i.e., the height of our hypothetical tensile specimen), changing the value of h in Equation 2. Second, rigid filler would further reduce the effective gage length of material capable of deforming in our hypothetical tensile specimen. Third, fibre constraint and or debonding could change the local strain to fracture. These three factors could potentially account for the decrease in fracture toughness from $8100 J/m^2$ in the F185 resin to $1900 J/m^2$ in the composite delamination fracture toughness. The first two of these three factors can be quantified based on actual observations. If one assumes that microcracking begins for strains above a threshold strain, then the extent of the microcracked zone can be used to quantify the magnitude of the h in Equation 2.

A cross-section of the composite prepared metallographically to reveal the microstructure (Figure 8) may be used to determine the volume fraction of fibres in the hypothetical tensile specimen ahead of the crack tip. Since the volume fraction is quite nonuniform, the

microstructure was divided into three regions: the resin rich region between plies with a fibre volume fraction of 19%; the ply region with a volume fraction of fibres of 76% and a transition zone with a volume fraction of approximately 33%. The relative heights of these three regions are shown in the schematic in Figure 8, along with the height of the microcracked zone in the F185 resin. Using a simple rule of mixtures approach, and taking account of the smaller microcracked (and deformed) zone, one may estimate the delamination fracture toughness to be 4000J/m^2 as shown below:

$$G_{Ic} = \frac{J_{Ic}}{h_0} \left[h_A (1-V^A_f) + h_B (1-V^B_f) + h_c (1-V^C_f) \right]$$

This calculation implicitly assumes that the local strain to fracture in the F185 resin and the composite are the same and that the stress distribution is also similar, at least on the average.

Since the measured value of delamination fracture toughness in this system is 1900 J/m^2 , the estimated value of 4000J/m^2 is seen to be quite excessive. It also strongly suggests what the in-situ fractograph has already indicated; namely, that preferential microcrack nucleation at the fibre/resin interface leads to premature failure, preventing the realization of 4000J/m^2 that might otherwise be possible. This suggests that more attention to the interphase region is required if a greater fraction of the intrinsic toughness of the neat resin is to be manifested in delamination fracture toughness of the fibre reinforced composite material.

SUMMARY

1. The delamination fracture toughness of the T6T145/F185 composite is 1900 J/m^2 whereas the fracture toughness of the neat F185 resin is 8100 J/m^2.
2. Microcracking in the resin appears to be a significant deformation mode for load redistribution at the crack tip.
3. Crack progagation occurs in a discontinuous manner through microcrack coalescence ahead of the crack tip.
4. In the composite, the microcracking is coarser and coalescence seems to occur preferentially at the resin-fibre interface.
5. The height of the deformation zone, above and below the plane of crack propagation, is greater in the resin than in the composite.
6. Comparison of the relative heights of the damage zone yielded 4000 J/m^2 as a calculated delamination G_{Ic} for the composite, which is an over-estimation by a factor of two.
7. It may be inferred that the strain to failure in the composite is lowered, probably due to premature microcrack coalescence at the resin fibre interface.

ACKNOWLEDGEMENTS

The authors wish to acknowledge the generous financial support of both the National Aeronautics and Space Administration, Langley Research Center, (Dr. John Crews, Project Monitor) and the Air Force Office of Scientific Research (Major David Glasgow, Project Monitor). Special thanks are due Laurie Veeder for her careful macroscopic testing.

REFERENCES

1. C.K. Riew, E.H. Rowe, and A.[illegible]ert, "Toughness and Brittleness of Plastics," R.D. Deanin and [illegible]. Crugnola, Eds., Adv. Chem. Ser. No. 154, Am. Chem. Soc., Washington, D.C., 1976, p. 326.

2. W.D. Bascom, R.Y. Ting, R.J. Moulton, C.K. Riew and A.R. Siebert, J. Maker. Sci., 16 , 2657 (1981).

3. L.T. Manzione and J.K. Gillham, J. Appl. Polym. Sci., 26 , 890 (1981).

4. L.T. Manzione and J.K. Gillham, J. Appl. Ploym. Sci., 26 , 907 (1981).

5. A.F. Yee and R.A. Pearson, "Toughening Mechanism in Elastomer - Modified Epoxy Resins - Part 1", NASA Contractor Report 3718, NASA Scientific and Technical Information Branch, Washington, D.C., (1983).

6. A.F. Yee and R.A. Pearson, "Toughening Mechanism in Elastomer - Modified Epoxy Resins - Part II", NASA Contractor Report 3852, NASA Scientific and Technical Information Branch, Washington, D.C., (1984).

7. W.D. Bascom, J.L. Bitner, R.J. Moulton and A.R. Siebert, Composites , ii, 9 (1980).

8. W.L. Bradley and R.N. Cohen, "Matrix Deformation and Fracture in Graphite Reinforced Epoxies", ASTM Symposium on "Delamination and Debonding in Materials", Pittsburgh, Nov. 1983.

9. W.L. Bradley and R.N. Cohen, "Delamination and Transverse Fracture in Graphite/Epoxy Materials", Fourth Internat. Conf. on Mech. Behavior of Mater., Stockholm, Sweden, August 1983.

10. W.M. Jordan, Ph.D Thesis, Interdisciplinary Engineering, Texas A&M University, College Station, TX, (1985).

11. Specification sheet for F185 resin from Hexcel Corporation.

12. D.F. Devitt, R.A. Schapery and W.L. Bradley, Composite Mater. 14 , 270 (1980).

List of Nomenclature

B	Width of double cantilever beam specimen
E	Elastic modulus in the fibre direction
ε_{ij}	Failure strain for strain component
G_{Ic}	Delamination fracture toughness under Mode I loading
h	Height of damage zone above the plane of crack propagation (2h = total height)
h_0	Same as above for resin
h_A, h_B, h_C	Same as above for the composite in regions of differing fibre volume fraction
I	Moment of inertia of one half of the DCB specimen
J	Resin fracture toughness under Mode I loading
L	Crack length (equivalent beam length for linear beam analysis)
σ_{ij}	Component to stress tensor representing stress in hypothetical tensile bar (see Fig. 7)
P	Load applied to split laminate

FIGURES

1. Load-displacement record for [illegible]mpact tension specimen of F185 resin showing considerable no[illegible]nearity.

2. Microcracking ahead of the crack tip in F185 resin showing crack growth sequence under a constant applied displacement.
   (a) 1500x. Shape of the damage zone. Arrow markers correspond to regions similarly marked in Figure 2(e).

   (b) 3000x. Detail of crack tip. Arrow markers here correspond to similarly marked regions in Figures 2(c) and 2(d).

   (c) 900x. Crack propagation through microcrack coalescence to form a very sharp narrow crack.

   (d) 5000x. Crack extension of about 22 m. New crack tip is very sharp.

   (e) 1000x. Blunting of new crack tip with development of damage zone ahead of the tip. Total crack growth in the sequence is about 140 m (compare with Figure 2(a)).

3. Microcracking ahead of the crack tip in AS4/3502 at 3000x.
   (a) coated prior to loading
   (b) coated after loading

4. Fracture surface of F185 resin. Crack growth is from left to right.

   (a) 330x. Away from the free surface. Arrows indicate a lip formed by crack tip blunting after a growth sequence.

   (b) 330x. Just adjacent to the free surface.

   (c) 10,000x. Detail of a relatively flat region in (a). cavitation due to phase separated CTBN. Facets separated by ledges probably correspond to microcrack coalescence.

5. 1000x. In situ delamination of T6T145/F185 composite showing microcracking in the damage zone ahead of the crack tip. Note microcracking is more dense adjacent to the fibres. Preferential microcrack coalescence near the resin fibre interface where the micorcracks are inclined to the primary crack.

6. Fracture surface of T6T145/F185 composite.
   (a) 3000x. Higher density of cavitation adjacent to fibres.

   (b) 4500x. Scalloped appearance of resin between fibres from coalescence of inclined microcracks near resin-fibre interface.
   (c) 10,000x. Voiding adjacent to solid pre-reacted rubber

particles. Comparison with Figure 3 (c) shows that the cavitation due to phase separated CTBN is much coarser here than in the neat F185 re[illegible]

7. Schematic of hypothetical tensile bar ahead of the crack tip with the strain distribution accross it.
8. 600x. Cross section of T6T145/F185 showing interlaminar resin rich region.

9. Schematic showing relative height of damage zone in F185 resin and T6T145/F185 composite.

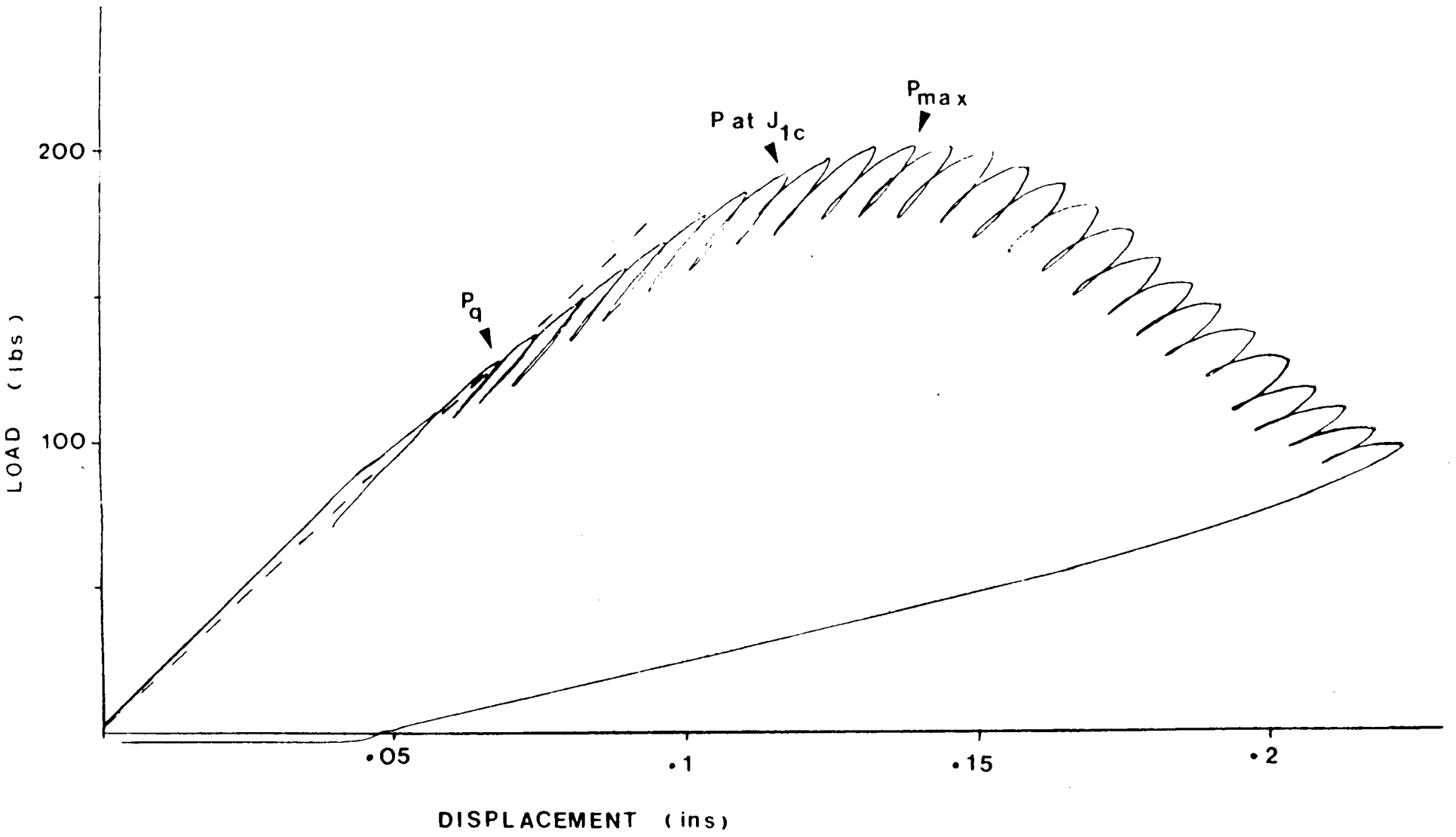
200
100
LOAD (lbs)
P_q
P at J_{1c}
P_{max}
•05
•1
•15
•2
DISPLACEMENT (ins)

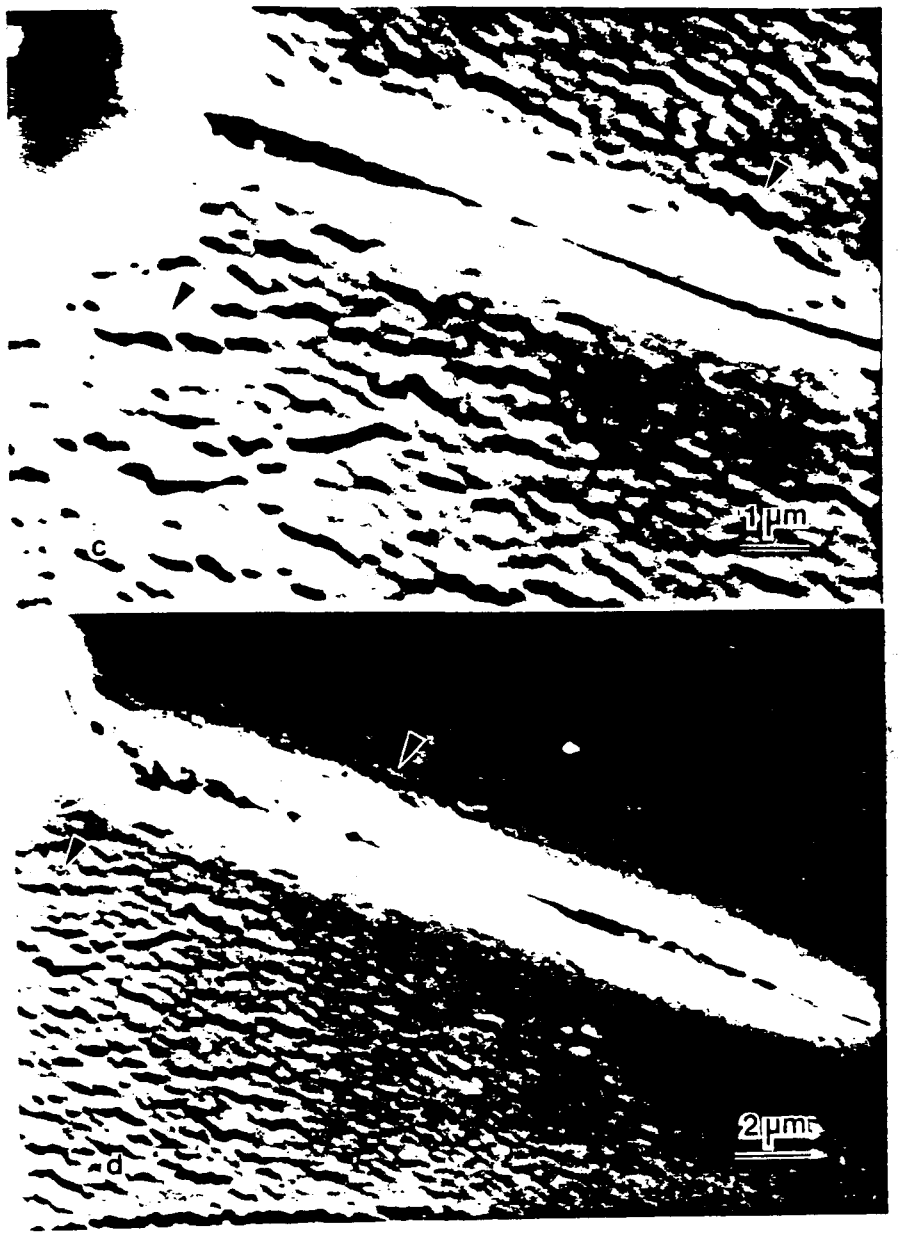

e
10 µm

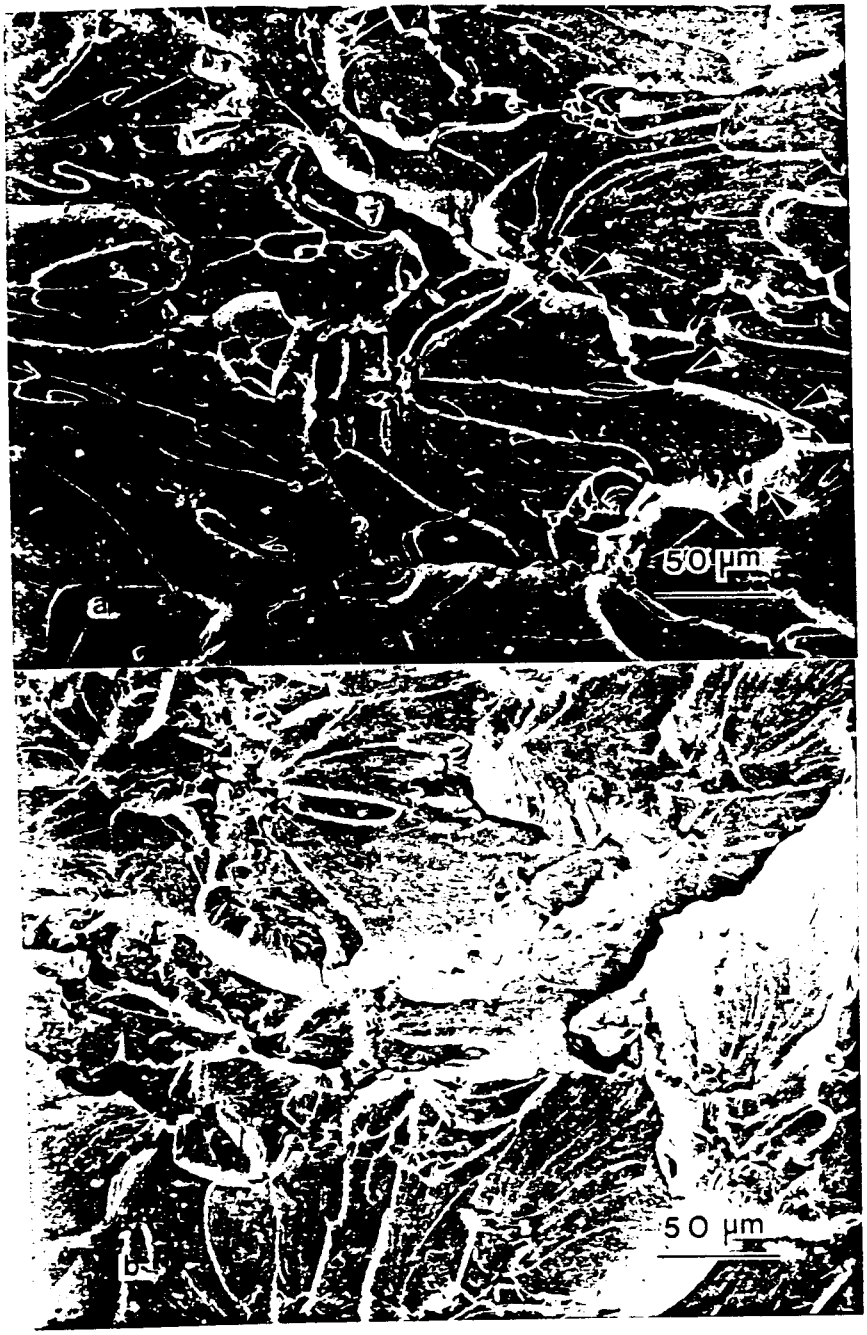

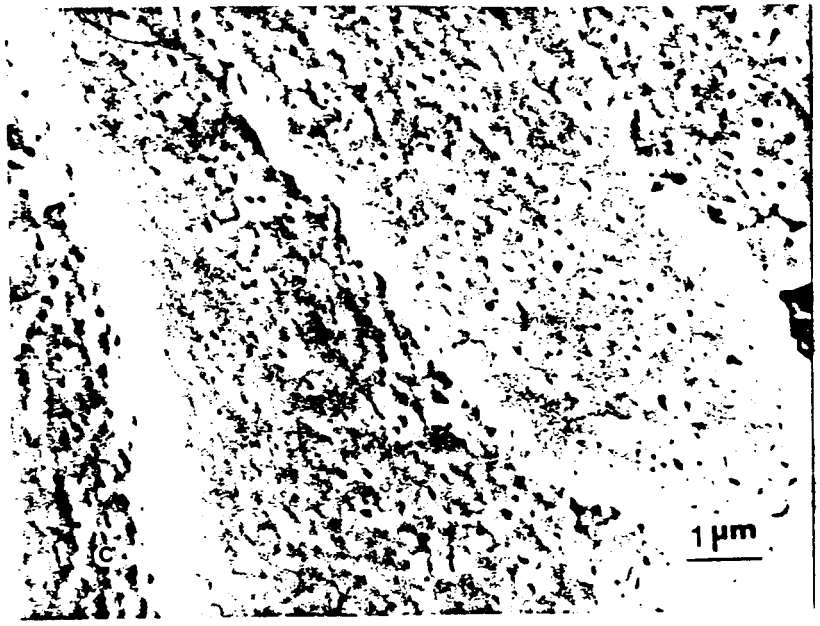

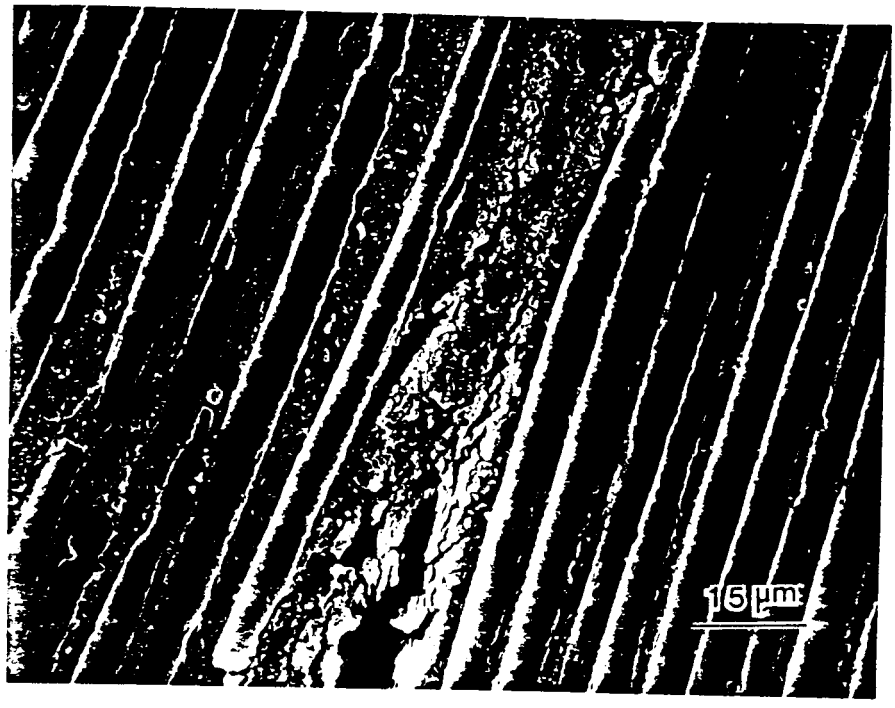

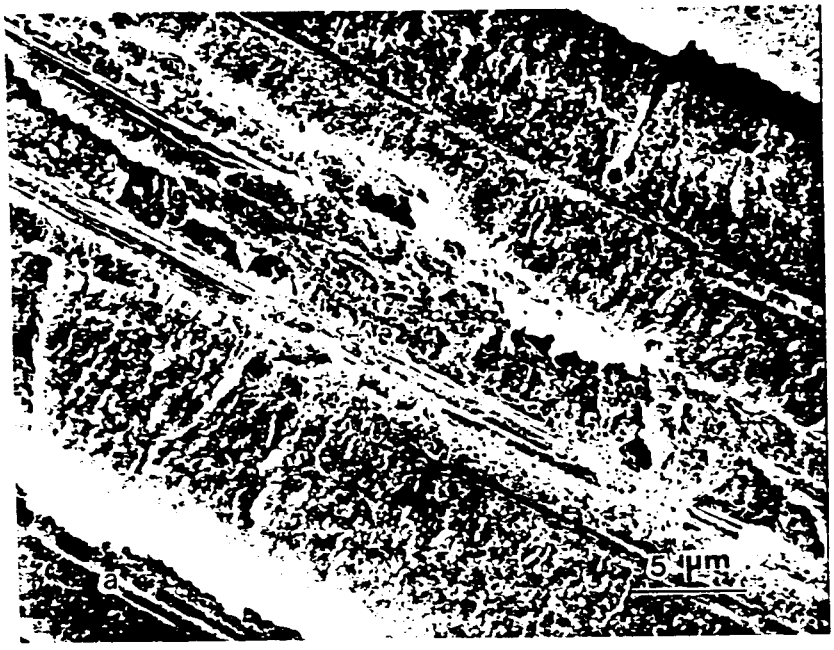
a
5 µm

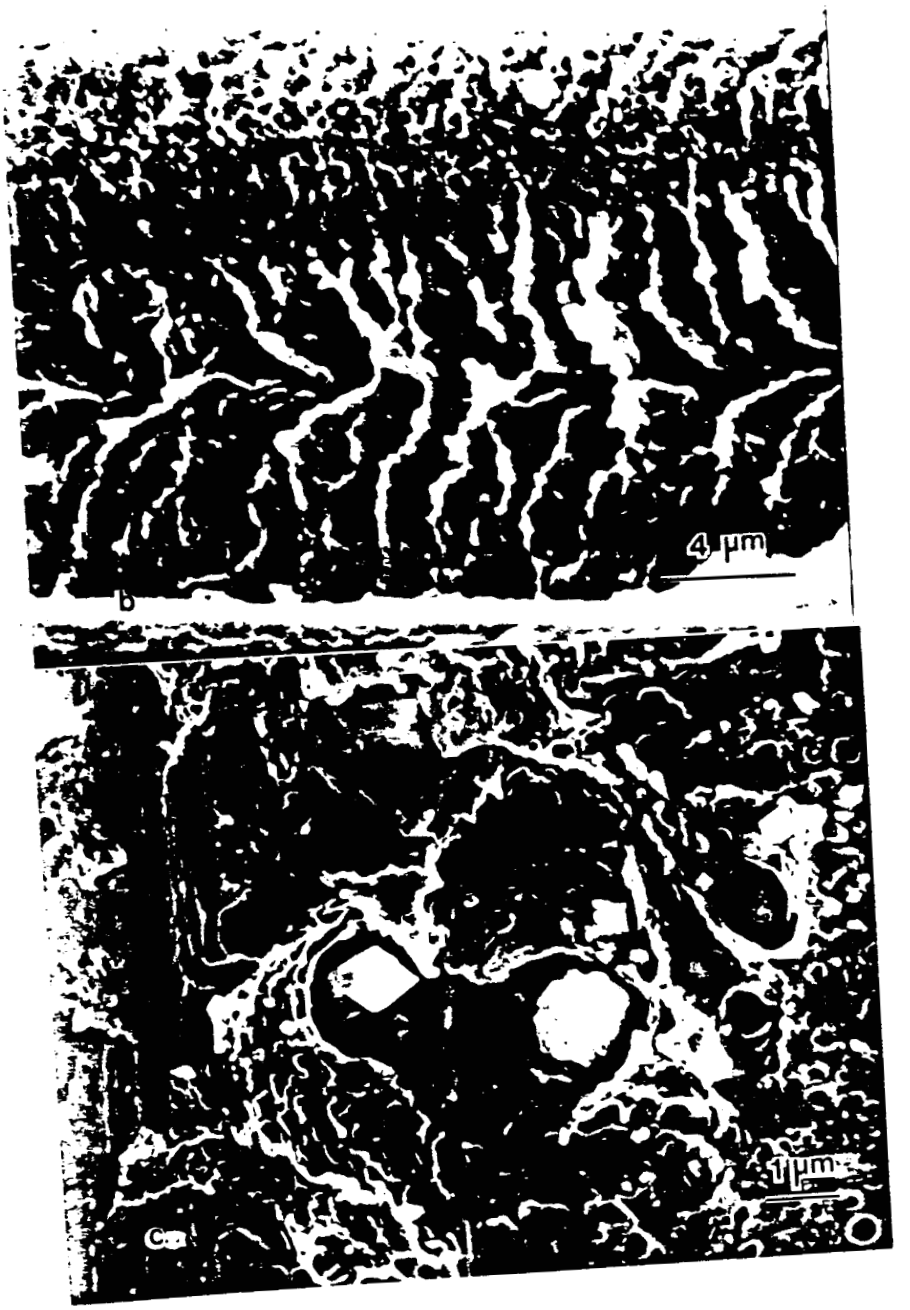

$$G_{Ic} = \int_{-h}^{h} \int_{0}^{\varepsilon_{ij}} \sigma_{ij} \, d\varepsilon_{ij} \, dy$$

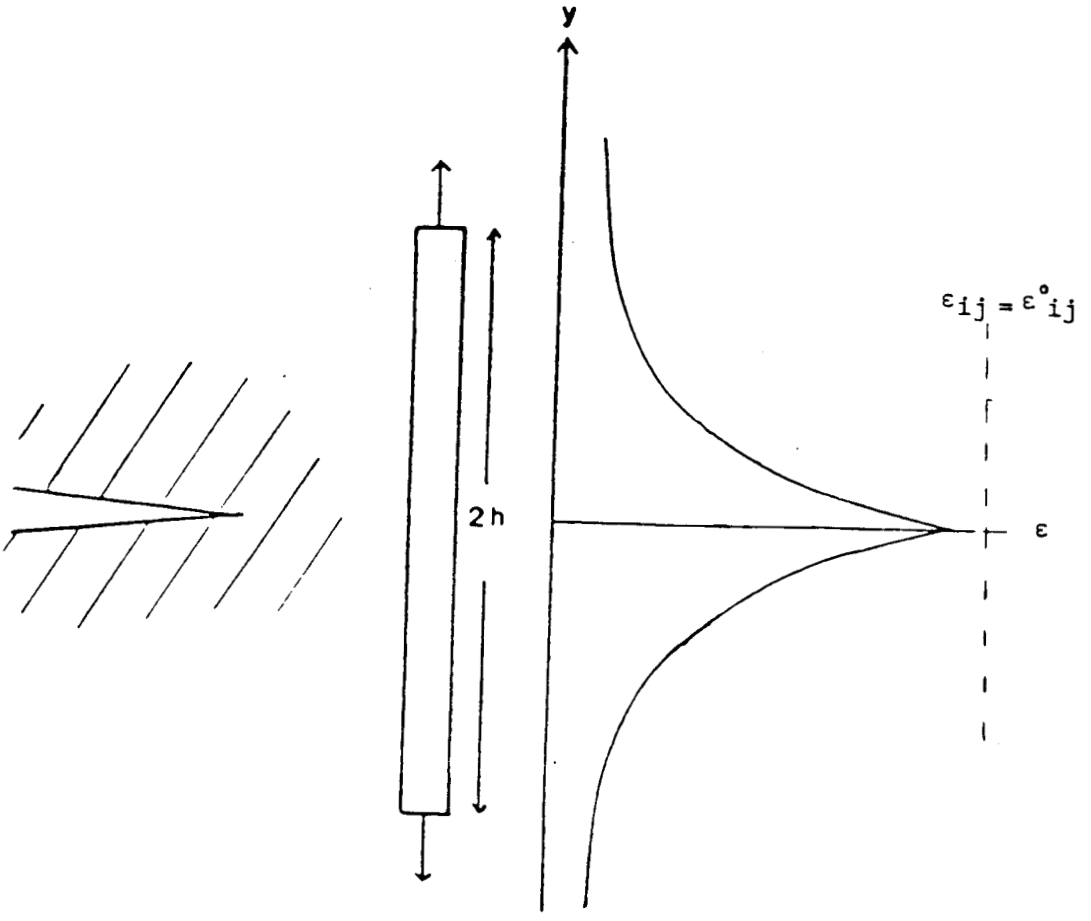

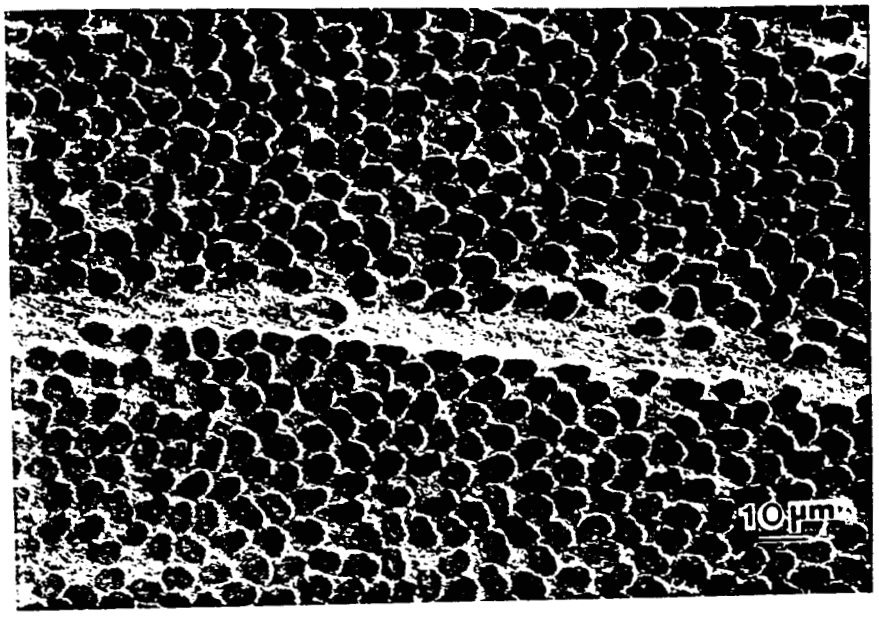

$$G_{Ic} \int_{-h}^{h} \int_{0}^{\varepsilon_{ij}} \sigma_{ij} \, d\varepsilon_{ij} \, dy$$

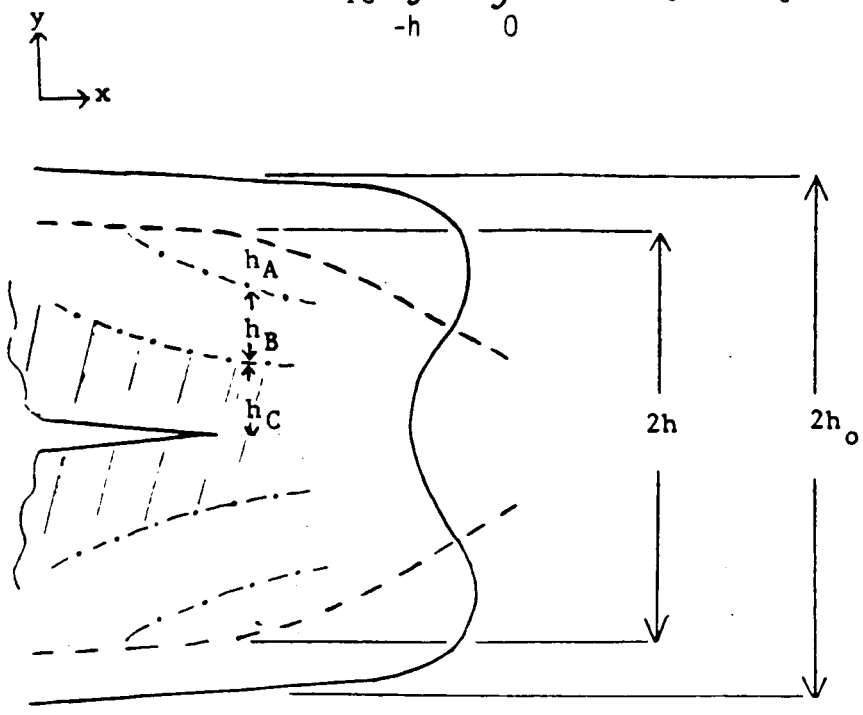

———	resin	$2h_o$	130 µm
– – – –	composite	2h	100 µm